

# A Field Theoretical Approach to the Quasi-Continuum Method

Mrinal Iyer, Vikram Gavini \*

*Department of Mechanical Engineering, University of Michigan, Ann Arbor, MI 48109, USA*

---

## Abstract

The quasi-continuum method has provided many insights into the behavior of lattice defects in the past decade. However, recent numerical analysis suggests that the approximations introduced in various formulations of the quasi-continuum method lead to inconsistencies—namely, appearance of ghost forces or residual forces, non-conservative nature of approximate forces, etc.—which affect the numerical accuracy and stability of the method. In this work, we identify the source of these errors to be the incompatibility of using quadrature rules, which is a local notion, on a non-local representation of energy. We eliminate these errors by first reformulating the extended interatomic interactions into a local variational problem that describes the energy of a system via potential fields. We subsequently introduce the quasi-continuum reduction of these potential fields using an adaptive finite-element discretization of the formulation. We demonstrate that the present formulation resolves the inconsistencies present in previous formulations of the quasi-continuum method, and show using numerical examples the remarkable improvement in the accuracy of solutions. Further, this field theoretic formulation of quasi-continuum method makes mathematical analysis of the method more amenable using functional analysis and homogenization theories.

*Key words:* Quasicontinuum method, Atomistic Models, Error analysis, Multiscale modeling

---

## 1 Introduction

Deformation and failure processes in crystalline solids are strongly governed by the properties of various defects present in them—examples include the role of vacancies in creep, spalling and radiation damage, dislocations in metal plasticity, twin boundaries in phase-transformations, and interfaces in reactive metals. The main challenge in an

---

\* Corresponding Author ([vikramg@umich.edu](mailto:vikramg@umich.edu))

accurate description of defect behavior is the wide range of interacting length-scales that determine the properties of defects. The core of a defect is determined by complex atomistic/quantum-mechanical interactions on an Angstrom length-scale, which in turn produces long-ranged elastic fields over many micrometers. The Quasi-continuum method is a numerical coarse-graining technique that attempts to bridge these various length-scales to accurately describe defect behavior in solids. We refer to the following articles and references therein for a comprehensive overview of the quasi-continuum method and its applications: [Tadmor et al. \(1996a,b\)](#); [Miller et al. \(1998a,b\)](#); [Phillips et al. \(1999\)](#); [Ortiz & Phillips \(1999\)](#); [Tadmor et al. \(1999\)](#); [Shenoy et al. \(2000\)](#); [Knap & Ortiz \(2001\)](#); [Miller & Tadmor \(2002\)](#); [Knap & Ortiz \(2003\)](#); [Curtin & Miller \(2003\)](#); [Gavini et al. \(2007\)](#); [Eidel & Stukowski \(2009\)](#).

The quasi-continuum (QC) method was originally developed in the context of lattice statics at zero temperature using empirical interatomic potentials ([Tadmor et al. , 1996a,b](#)), where the key idea was the systematic and adaptive coarse-graining from a fully resolved atomistic description near a defect-core to a continuum description away from the core. This was achieved through kinematic constraints on the degrees of freedom—positions of atoms, thus reducing the variational problem of computing the ground-state properties to a constrained variational problem with far fewer degrees of freedom. Although the imposed kinematic constraints significantly reduce the number of variables, the computational complexity of evaluating the generalized forces corresponding to the coarse-grained variables—positions of representative atoms—still scales with the total number of atoms in the system making computations on large systems intractable.

Various approximations have been suggested to further reduce the complexity of force computations and make it commensurate with the number of coarse-grained variables ([Tadmor et al. , 1996a,b](#); [Shenoy et al., 1999](#); [Knap & Ortiz, 2001](#); [Miller & Tadmor, 2002](#); [Eidel & Stukowski, 2009](#)). These include the mixed atomistic and continuum formulations, or introduction of cluster summation rules on lattice sums. Valuable as these approximations are, they suffer from notable drawbacks. In some cases, the computed forces are non-conservative which may lead to energy conservation problems as studied in [Shimokawa et al. \(2004\)](#). In other cases, where the computed forces are conservative, spurious forces appear as a result of the approximations introduced and can undermine the accuracy of the solution. Many strategies have been suggested to correct the errors incurred in these approximations (cf. e.g. [Shimokawa et al. \(2004\)](#); [E et al. \(2006\)](#)), but these require a special treatment at the interfaces separating the heterogeneous models used in different regions of the materials system, and subsequently introduce a seam in the formulation. Recently, many efforts have focussed on a systematic numerical analysis to investigate the accuracy, consistency and stability of the various approximations in the quasi-continuum method, and we refer to [E et al. \(2006\)](#); [Dobson & Luskin \(2009\)](#); [Dobson et al. \(2009\)](#); [Ming & Yang \(2009\)](#); [Luskin & Ortner \(2009\)](#); [Dobson et al. \(2010a,b\)](#) and reference therein for a detailed discussion on this topic.

In the present work, we seek to construct a seamless quasi-continuum formulation which

is solely based on a single theory, is variational, and provides systematic convergence of the approximations introduced. The notion of cluster summation rules introduced in [Knap & Ortiz \(2001\)](#); [Eidel & Stukowski \(2009\)](#) is attractive from the standpoint of being a seamless formulation based on a single theory. However, the formulations based on this approximation are either not variational, or are not consistent as they fail the patch test. Moreover, these formulations can result in large errors and may not guarantee a systematic convergence of approximations. This was first noted in a recent analysis by [Luskin & Ortner \(2009\)](#). We further demonstrate this through the error estimates we compute in section 3. We identify the primary cause of these shortcomings to be the use of quadrature rules (cluster summation rules), which is a local notion of numerical approximation, on a non-local representation of energy describing the extended interatomic interactions. Further, this non-local representation of energy is also the cause for spurious ghost forces observed in the formulation proposed in [Tadmor et al. \(1996b\)](#), and subsequently discussed in [Shenoy et al. \(1999\)](#).

In this work, we first reformulate the non-local interatomic potentials into a local form by constructing the partial differential equation whose Green's function corresponds to the kernel of the non-local interaction. Most interatomic potentials are based on either an exponential kernel of the form  $e^{-\alpha|\mathbf{r}-\mathbf{r}'|}$ , or kernels of the form  $\frac{1}{|\mathbf{r}-\mathbf{r}'|^m}$  where  $m$  is a positive integer. We note that  $e^{-\alpha|\mathbf{r}-\mathbf{r}'|}$  is the Green's function of a 4th order partial differential equation, and show that kernels of the form  $\frac{1}{|\mathbf{r}-\mathbf{r}'|^m}$  can be approximated with Green's functions of Helmholtz equations without significant loss of accuracy. Thus, the extended interactions for a large class of interatomic potentials can now be described by a local variational problem involving potential fields, and this forms the basis for the field approach to the quasi-continuum method. In particular, as will be demonstrated in this article, the computation of energy as well as the physical forces on atoms reduce to local evaluations involving potential fields.

Following [Gavini et al. \(2007\)](#), the quasi-continuum reduction is performed on the potential fields which are governed by a local variational problem. The potential fields are first decomposed into predictor fields and corrector fields. The predictor fields are constructed from local periodic calculations using the Cauchy-Born rule. The corrector fields, which are represented on a coarse-grained triangulation, are then computed from the variational principle. In a related work ([Gavini & Liu, 2010](#)), we show that the corrector fields do not exhibit oscillations on the length-scale of the atomic lattice which justifies the computation of corrector fields on coarse-grained triangulations. Owing to the local nature of the formulation, we proceed to introduce quadrature rules that reduce all computations to have a complexity commensurate with the number of coarse-grained variables. We show that the quadrature rules introduced on this local variational problem satisfy the necessary consistency conditions for systematic convergence of approximations, which is one of the central results of this work.

To demonstrate the accuracy of the proposed field formulation of QC method we have numerically implemented the formulation using Morse potential. We compare the numerical results from the proposed formulation with other seamless QC formulations em-

ploying node-based cluster rules (Knap & Ortiz, 2001; Eidel & Stukowski, 2009) using a nanoindentation test problem in one dimension. We find that errors arising from quadrature approximations are almost negligible in the field formulation, and the approximation errors are predominantly coarse-graining errors associated with the kinematic constraints on positions of atoms which can not be surpassed in any QC formulation. These results are in sharp contrast to the approximation errors incurred when cluster summation rules are introduced on a non-local representation of the energy. In such a case, the quadrature errors are orders of magnitude larger than coarse-graining errors, and numerical results suggest a lack of systematic convergence with increasing number of representative atoms. These numerical results support our observations from error estimates in section 3, and highlight the strict control and systematic convergence afforded by the field approach to QC method. We further note that the field approach makes mathematical analysis of QC formulation more amenable, where established techniques from functional analysis and homogenization theories can be employed. A related work (Gavini & Liu, 2010) presents such an analysis.

The remainder of this article is organized as follows. Section 2 provides an overview of the QC method and briefly discusses the merits and demerits of different QC formulations. In particular, it highlights the issues involved in using quadrature rules on non-local representations of energy and motivates the main ideas developed in this work. Section 3 presents error estimates on forces and energy upon using cluster summation rules, and demonstrates the lack of consistency in these numerical approximations. Section 4 presents the reformulation of the extended interatomic interactions into local variational field theories, and section 5 presents the quasi-continuum reduction of these field theories and an analysis of the approximations therein. Numerical examples are presented in section 6, and we conclude in section 7 with an outlook.

## 2 Overview

We consider the reference configuration of a single crystallite, where the positions of the  $N_0$  atoms present in the crystallite are given by a subset of a simple Bravais lattice in a  $d$  dimensional space denoted by  $\mathcal{L}$ . Let  $\mathbf{l} = \{l^1, \dots, l^d\} \in \mathbb{Z}^d$  denote the lattice coordinates representing an individual atom. The coordinates of atoms in the reference configuration are thus given by

$$\mathbf{X}_{\mathbf{l}} = \sum_{i=1}^d l^i \mathbf{a}_i, \quad \mathbf{l} \in \mathcal{L}, \quad (1)$$

where  $\mathbf{a}_i$  for  $i = 1, \dots, d$  denote the basis vectors of the Bravais lattice. We denote by  $\mathbf{q} = \{\mathbf{x}_{\mathbf{l}}, \mathbf{l} \in \mathcal{L}\}$  a vector that collects the positions of atoms in the deformed configuration. The energy of a material system in atomistic calculations is given by

$$\Pi(\mathbf{q}) = E(\mathbf{q}) + V(\mathbf{q}), \quad (2)$$

where  $\Pi$  denotes the total potential energy of the system,  $E$  denotes the internal energy of the system, and  $V$  denotes the potential energy corresponding to body forces acting on the material system. The problem of computing ground-state properties, which include the ground-state energy and the deformed configuration, can now be expressed as the following variational problem:

$$\min_{\mathbf{q} \in X} \Pi(\mathbf{q}), \quad (3)$$

where  $X$  denotes the vector space of admissible trial functions corresponding to imposed boundary conditions. We note that the above minimization problem may not have a unique minimizer owing to the non-convex nature of the potential energy function. However, in most numerical simulations the crystallite is loaded incrementally in a quasi-static manner allowing the system to relax to a nearby stable configuration.

The internal energy of the system in atomistic calculations is often described by empirical interatomic potentials, the most common being the embedded atom method (cf. e. g. [Daw & Baskes \(1984\)](#)), and has a representation given by

$$E(\mathbf{q}) = \sum_{\mathbf{k} \in \mathcal{L}} \varepsilon_{\mathbf{k}}(\mathbf{q}), \quad (4a)$$

$$\varepsilon_{\mathbf{k}}(\mathbf{q}) = \sum_{\mathbf{j} \in \mathcal{L}, \mathbf{j} \neq \mathbf{k}} \bar{K}(|\mathbf{x}_{\mathbf{k}} - \mathbf{x}_{\mathbf{j}}|) + f(\bar{\rho}(\mathbf{k})) \quad \text{with} \quad (4b)$$

$$\bar{\rho}(\mathbf{k}) = \sum_{\mathbf{j} \in \mathcal{L}, \mathbf{j} \neq \mathbf{k}} \rho(|\mathbf{x}_{\mathbf{k}} - \mathbf{x}_{\mathbf{j}}|). \quad (4c)$$

In the above expression,  $\varepsilon_{\mathbf{k}}(\mathbf{q})$  denotes the internal energy of atom  $\mathbf{k}$ ,  $\bar{K}$  denotes a central potential governing the interatomic interactions,  $f$  denotes the embedding energy function and  $\bar{\rho}(\mathbf{k})$  denotes the electron density at atom  $\mathbf{k}$  in the environment of surrounding atoms. The ground-state properties corresponding to the variational problem in equation (3) are computed by equilibrating the forces on atoms given by

$$\mathbf{f}_{\mathbf{k}}(\mathbf{q}) = -\frac{\partial \Pi(\mathbf{q})}{\partial \mathbf{x}_{\mathbf{k}}} \quad \mathbf{k} \in \mathcal{L}. \quad (5)$$

Due to the non-convex nature of the energy functional, there may exist many solutions which satisfy  $\mathbf{f}_{\mathbf{k}} = 0$  for  $\mathbf{k} \in \mathcal{L}$ , and the ground-state properties correspond to the solution with minimum energy. In practice, the huge computational cost associated with an all-atom calculation limits the size of accessible material systems. However, the nature of deformation fields in most systems of interest, especially those involving defects, is such that these fields are rapidly varying only near the core of a defect, and become smooth away from the core where the response is effectively elastic. This nature of deformation fields is the basis for the quasi-continuum method, which is an adaptive numerical coarse-graining technique retaining full resolution where necessary and coarse-graining elsewhere.

A key idea behind quasi-continuum method is to replace the minimization problem in equation (3) with a constrained minimization problem in a suitably chosen sub-space. We consider a subset of *representative atoms* denoted by  $\mathcal{L}_h$  and construct a finite-element tri-

angulation  $T_h$  of these representative atoms in the reference configuration, which in general is unstructured. Further, kinematic constraints are introduced on positions of atoms in the deformed state through shape-functions of the finite-element triangulation given by

$$\mathbf{x}_k^h = \sum_{\mathbf{J} \in \mathcal{L}_h} \Phi^h(\mathbf{X}_k | \mathbf{X}_J) \mathbf{x}_J^h \quad \mathbf{k} \in \mathcal{L}, \quad (6)$$

where  $\Phi^h(\mathbf{X}_k | \mathbf{X}_J)$  denotes the value of the shape-function associated with a representative atom  $\mathbf{J}$  evaluated at the position of atom  $\mathbf{k}$  in the reference configuration. Let  $\mathbf{q}^h = \{\mathbf{x}_k^h, \mathbf{k} \in \mathcal{L}\}$  be a vector containing positions of atoms in the deformed configuration under the kinematic constraint imposed through equation (6). The energy of the system is now a function of positions of only the representative atoms, and the minimization problem in equation (3) reduces to a constrained minimization problem given by

$$\min_{\mathbf{q}^h \in X_h} \Pi(\mathbf{q}^h), \quad (7)$$

where  $X_h$  denotes the subspace of  $X$  spanned by the shape-functions of the finite-element triangulation. A judicious choice of the subspace  $X_h$  corresponds to providing full atomistic resolution in regions of rapidly varying deformation fields, for example at the defect-core, and using fewer representative nodes in regions of smooth deformations. Many numerical tests (cf. e. g. [Tadmor et al. \(1996a\)](#); [Knap & Ortiz \(2001\)](#)) have shown that the ground-state properties of a system can be represented by the constrained minimization problem in equation (7), which has far fewer degrees of freedom than equation (3).

The force on a representative atom at  $\mathbf{J} \in \mathcal{L}_h$  is given by

$$\begin{aligned} \mathbf{f}_J^h(\mathbf{q}^h) &= -\frac{d\Pi(\mathbf{q}^h)}{d\mathbf{x}_J^h} = -\sum_{\mathbf{k} \in \mathcal{L}} \frac{\partial \Pi(\mathbf{q}^h)}{\partial \mathbf{x}_k^h} \frac{\partial \mathbf{x}_k^h}{\partial \mathbf{x}_J^h} \\ &= \sum_{\mathbf{k} \in \mathcal{L}} \mathbf{f}_k(\mathbf{q}^h) \Phi^h(\mathbf{X}_k | \mathbf{X}_J), \end{aligned} \quad (8)$$

which is a weighted sum of forces on atoms that lie in the compact support of the shape-function associated with representative atom  $\mathbf{J}$ . Thus, although the kinematic constraints introduced in the quasi-continuum method significantly reduce the degrees of freedom, forces on all atoms in the system are required to compute forces on representative atoms. A full atomistic force calculation is prohibitively expensive on large systems and further approximations are necessary to reduce the computational complexity of these force calculations. We note that the kinematic constraints introduced through the selection of representative atoms is common to all versions of the quasi-continuum method developed so far (cf. e. g. [Tadmor et al. \(1996a\)](#); [Shenoy et al. \(1999\)](#); [Knap & Ortiz \(2001\)](#); [Miller & Tadmor \(2002\)](#); [Eidel & Stukowski \(2009\)](#)). The various versions of the method differ in the next approximation which is introduced to reduce the computational complexity of the force calculation. Here we briefly discuss and comment on the merits and demerits of commonly used formulations proposed in [Tadmor et al. \(1996a\)](#) and [Knap & Ortiz \(2001\)](#), and a recent formulation proposed in [Eidel & Stukowski \(2009\)](#).

In the first formulation of quasi-continuum method, proposed in [Tadmor et al. \(1996a\)](#), the domain of analysis was divided into two regions—the non-local region where the energy is described by empirical interatomic potentials with extended interactions, and the local region where the energy is described by invoking the Cauchy-Born rule. The force computations are expensive only in the non-local region which is small compared to the local region, thus reducing the computational complexity of the calculation. However, the heterogeneous and disparate models used in different regions of the domain result in spurious forces on the interface between the local and the non-local region, and are often referred to as *ghost forces* in the literature. [Shenoy et al. \(1999\)](#) proposed to remove the effect of these ghost forces by adding a dead load which is the negative of these ghost forces. But the drawback of this approach is that these dead loads are non-conservative and may lead to energy conservation problems ([Shimokawa et al., 2004](#)) in molecular dynamics simulations. [Shimokawa et al. \(2004\)](#); [E et al. \(2006\)](#) suggest a remedy to this problem by introducing a buffer region or using local reconstructions between the local and the non-local region, but in the process introduce undesirable seams in the formulation.

A seamless approach to reduce the computational complexity of the force calculations was proposed in [Knap & Ortiz \(2001\)](#). In the spirit of quadrature rules, the force computations are approximated by *cluster summation rules* that represent a weighted sampling of forces on atoms located in clusters centered at representative atoms. Although this formulation is free of ghost forces, the approximate forces are non-conservative ([Eidel & Stukowski, 2009](#)) which is not desirable as mentioned before. [Eidel & Stukowski \(2009\)](#) suggest introducing cluster summation rules only on the energy, and computing the forces on representative atoms as tangents of this approximate energy. However, this leads to the appearance of non-zero residual forces for a perfect crystal under affine deformations. These residual forces can become uncontrollably large for an arbitrary coarse-graining of representative nodes as will be demonstrated in section 3.2, and in turn can produce a spurious displacement field upon relaxation. It is suggested in [Eidel & Stukowski \(2009\)](#) that these residual forces can be eliminated by introducing dead loads on similar lines as proposed in [Shenoy et al. \(1999\)](#). The difference between ghost forces in [Tadmor et al. \(1996a\)](#) and the residual forces in [Eidel & Stukowski \(2009\)](#) is that the former are non-conservative while the latter are conservative. We note that the calculation of residual forces in [Eidel & Stukowski \(2009\)](#) requires evaluation of exact forces periodically, which is prohibitively expensive. Furthermore, we demonstrate in this article through numerical examples that the self-consistent iterations may not always converge (cf. section 6.1).

The introduction of cluster summation rules in [Knap & Ortiz \(2001\)](#) and [Eidel & Stukowski \(2009\)](#) in the spirit of quadrature rules is based on systematic numerical approximation, in contrast to the formulation proposed in [Tadmor et al. \(1996a\)](#) and its subsequent improvements ([Shenoy et al., 1999](#); [Shimokawa et al., 2004](#); [E et al., 2006](#)) where different regions of the model are described by heterogeneous theories. However, numerical examples in a bench mark test conducted recently ([Miller & Tadmor, 2009](#)) show that errors in the node-based cluster formulations ([Knap & Ortiz, 2001](#); [Eidel & Stukowski, 2009](#)) are considerably larger than other formulations. A recent analysis by [Luskin & Ortner \(2009\)](#)

based on nearest-neighbor interactions in one dimension (1D) provides an explanation for these observations, where they demonstrate using error analysis that node-based cluster rules can have large errors. In section 3, we estimate the errors in forces and energy using extended interactions and arrive at a similar conclusion. We further show that element-based cluster rules (Gunzburger & Zhang, 2009)—where the quadrature rules are introduced inside the element—exhibit better approximation properties for both forces and energy, and reduce to the Cauchy-Born rule for large elements in the leading order.

The next observation we present is the primary cause of the above mentioned inconsistencies in various versions of quasi-continuum method. We note that it is desirable to introduce cluster (quadrature) rules on the energy and compute forces as tangents of this approximate energy—this guarantees conservative forces. Further, any cluster rule introduced should satisfy the following necessary consistency conditions for systematic convergence (cf. e. g. Strang & Fix (1973); E et al. (2006)):

C1. The energy is summed exactly for affine deformations of perfect lattice.

C2. The computed forces—tangents of the energy—are zero for affine deformations of perfect lattice.

The consistency condition C2 is often referred to as *patch test* in numerical analysis of approximation theories. We remark that if the energy has a local representation, then the patch test is passed trivially. However, if the energy has a non-local representation then the patch test is never passed by a cluster rule of any order.

We consider the following example to illustrate this key point. As shown in figure 1, consider an infinite mono-atomic chain of atoms with uniform spacing between the atoms (affine deformation in 1D), and let  $\Omega$  denote the domain of analysis which consists of  $N_0$  atoms. First, we consider an artificial *local representation* for the energy given by a lattice function  $\varepsilon$ , where  $\varepsilon(i) = g(x_i)$  denotes the energy of atom  $i \in \mathcal{L}$  which is located at position  $x_i$ . A system of non-interacting atoms moving in a mean potential field ( $g(x)$ ) created by the atoms themselves has such a local representation for energy. Such a mean field representation is motivated from density functional theory (cf. e. g. Finnis (2003)), where it is used to account for the interaction between electrons. Using cluster summation rules the lattice sum describing the energy can be approximated as

$$E = \sum_{i \in \mathcal{L}} \varepsilon(i) \approx \sum_{k=1}^m n_k \sum_{i \in C_k} \varepsilon(i) = \tilde{E}, \quad (9)$$

where  $\tilde{E}$  denotes the approximate energy,  $C_k$  denotes the collection of atoms in the  $k^{\text{th}}$  cluster with a weight  $n_k$ , and  $m$  denotes the number of clusters. Similar to numerical approximation of integrals, the cluster weights and position of these clusters can be chosen such that the approximation is exact for polynomial lattice functions of order  $p$ —a  $p^{\text{th}}$  order accurate cluster rule. Now we consider the directional derivative of the energy for infinitesimal deformations  $\psi_\epsilon : \Omega \rightarrow \Omega$ , with  $\psi_0 = id$  and  $\frac{d\psi_\epsilon}{d\epsilon}|_{\epsilon=0} = \Gamma$  denoting the generator of these infinitesimal deformations. The generalized force is given by

$$f = \left. \frac{dE}{d\epsilon} \right|_{\epsilon=0} = \sum_{i \in \mathcal{L}} \left. \frac{d}{d\epsilon} \left\{ g(\psi_\epsilon(x_i)) \right\} \right|_{\epsilon=0} = \sum_{i \in \mathcal{L}} g'(x_i) \Gamma(x_i), \quad (10)$$

and the approximate generalized force, which is the directional derivative of  $\tilde{E}$ , is given by

$$\tilde{f} = \left. \frac{d\tilde{E}}{d\epsilon} \right|_{\epsilon=0} = \sum_{k=1}^m n_k \sum_{i \in C_k} \left. \frac{d}{d\epsilon} \left\{ g(\psi_\epsilon(x_i)) \right\} \right|_{\epsilon=0} = \sum_{k=1}^m n_k \sum_{i \in C_k} g'(x_i) \Gamma(x_i). \quad (11)$$

From translational invariance of the mono-atomic chain, we note that  $\varepsilon(i) = C$ , a constant, for  $i \in \mathcal{L}$ . Thus, a zeroth order cluster rule is sufficient to ensure that the energy is summed exactly (C1). Also, from symmetry,  $g'(x_i) = 0$  for  $i \in \mathcal{L}$  and the cluster rule immediately passes the patch test (C2).

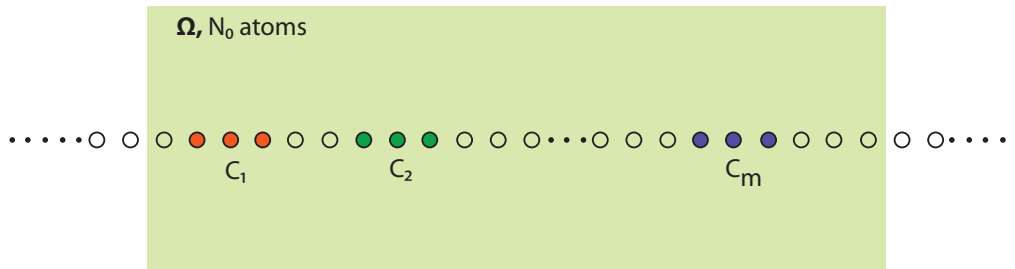


Fig. 1. Schematic of a 1D mono-atomic chain subjected to affine deformation. The circles in color are atomic-sites which belong to clusters.

Next, we will consider a *non-local* representation of the energy and demonstrate that a cluster rule of any order will not pass the patch test. Consider a non-local representation of energy given by

$$E = \sum_{i \in \mathcal{L}} \varepsilon(i), \quad \text{where} \quad (12a)$$

$$\varepsilon(i) = \sum_{\substack{j \in \mathcal{L} \\ j \neq i}} \bar{K}(|x_i - x_j|) \quad (12b)$$

and  $\bar{K}$  denotes the kernel representing extended interatomic interactions. The approximate energy is still given by equation (9), where a zeroth order quadrature rule is sufficient to ensure the consistency condition on energy (C1). The approximate generalized force for this non-local representation of energy is given by

$$\tilde{f} = \sum_{k=1}^m n_k \sum_{i \in C_k} f_i \Gamma(x_i) + \sum_{j \in \mathcal{L}} \Gamma(x_j) \left\{ \sum_{k=1}^m n_k \sum_{\substack{i \in C_k \\ i \neq j}} \bar{K}'(|x_i - x_j|) \frac{x_j - x_i}{|x_j - x_i|} \right\}, \quad (13)$$

where  $f_i = \sum_{\substack{j \in \mathcal{L} \\ j \neq i}} \bar{K}'(|x_i - x_j|) \frac{x_i - x_j}{|x_j - x_i|}$ . From symmetry, we note that the first term in the above expression vanishes as  $f_i = 0$  for  $i \in \mathcal{L}$ . However, for arbitrary  $\Gamma$ , the second term will not vanish for a cluster rule of any order, unless these clusters overlap to cover the complete domain (also cf. [Eidel & Stukowski \(2009\)](#); [Luskin & Ortner \(2009\)](#) for discussion on this point). Error estimates derived in sections 3.2 and 3.3 to follow reinforce this key point. We note that this failure of patch test is not a deficiency of the cluster rules, but

the result of an inconsistency in adopting a local concept of quadrature rules on a non-local representation of energy. We resolve this key issue by reformulating the extended interatomic interactions into a local variational form by solving for potential fields corresponding to these interactions (section 4) and subsequently introduce the quasi-continuum reduction of these fields (section 5).

### 3 Error Estimates

We begin by establishing error estimates for node-based cluster summation rules used in Knap & Ortiz (2001) and Eidel & Stukowski (2009). Latter in this section we demonstrate that element-based cluster summation rules (Gunzburger & Zhang, 2009)—clusters present in the interior of finite-elements—are more accurate in comparison to node-based cluster rules. More importantly, we show through these error estimates that neither approximations are both conservative and consistent for an arbitrary coarse-graining of representative atoms, and thus a systematic convergence of these approximations can not be guaranteed.

We note that cluster summation rules are designed to be accurate in the fully resolved region of a triangulation of representative nodes and approximations are concentrated in the coarse-grained region of the triangulation where the clusters do not overlap. Further, as the focus is to understand the nature of these errors, we restrict our analysis to 1D where the estimates can be obtained in a form that will demonstrate the main attributes of these errors. To this end, we consider an infinite mono-atomic chain of atoms with differing deformation gradients,  $F_1$  and  $F_2$ , in the two semi-infinite half-chains (figure 2). We consider three representative nodes as shown in figure 2 and we are interested in the force on representative atom denoted as  $A$ , and the energy of atoms lying between representative atoms denoted as  $B$  and  $C$ . The representative nodes are chosen such that there are  $N$  atoms in element  $BA$  and  $Ny$  atoms in element  $AC$ , where  $y > 1$  denotes the rate of coarse-graining. The present construction is a simplified representation of the coarse-grained region in a quasi-continuum formulation, the difference being that deformations are in general different in elements lying to the left of  $B$  and right of  $C$ . To estimate the errors we further assume the following:

A1. The energy of the system is given  $E = \sum_{i \in \mathcal{L}} \sum_{\substack{j \in \mathcal{L} \\ j \neq i}} \bar{K}(|x_i - x_j|)$ , where the kernel  $\bar{K}(|x_i - x_j|)$  denotes a central potential representing extended interatomic interactions. Beyond a threshold distance  $r_{th}$ , measured in units of undeformed interatomic spacing  $a$ , the central potential has a decay given by  $\bar{K}(|x_i - x_j|) = \frac{1}{|x_i - x_j|^p}$ , where  $p$  is the decay exponent such that  $p > 2$ .

A2. The difference in deformation gradients in elements  $BA$  and  $AC$  is small— $F_1 \approx F_2$ . For convenience, we denote the interatomic spacing in  $AC$  (and to the right of  $C$ ) as  $a_1 = F_1 a$ , and the interatomic spacing in  $BA$  (and to the left of  $B$ ) as  $a_2 = F_2 a$ . Thus  $a_1 \approx a_2$ .

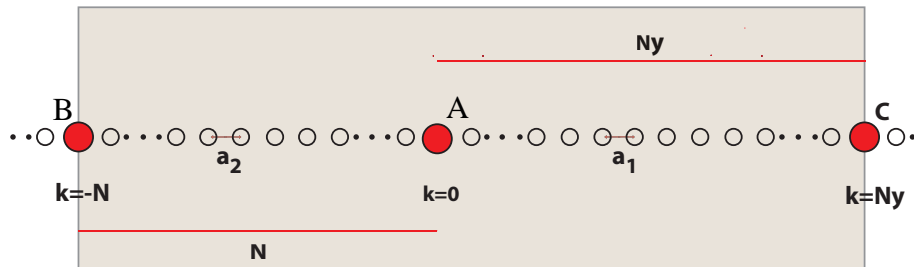


Fig. 2. Schematic of a coarse-grained region in 1D mono-atomic chain: circles denote atoms; circles in red denote representative atoms. Interatomic spacings in the semi-infinite half-chains to the right and left of  $A$  are  $a_1$  and  $a_2$  respectively.

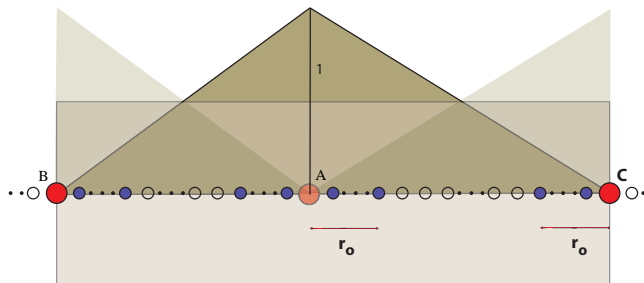


Fig. 3. Schematic of node-based cluster rules in 1D mono-atomic chain: circles in blue denote the atoms belonging to a cluster; shaded triangles represent the shape-functions of representative atoms restricted to the region  $BC$ .

A3. We consider  $N \gg r_0$ , where  $r_0$ , measured in units of undeformed interatomic spacing, is the radius of all clusters introduced in cluster summation rules. Further, we will assume  $r_0 \gg 1$  unless specified otherwise.

### 3.1 Node-based cluster rules for lattice sums

We first compute the errors in node-based cluster summations proposed in [Knap & Ortiz \(2001\)](#) where cluster rules are employed on lattice sums of both forces and energy independently. In node-based cluster formulations, clusters are centered at the representative nodes as shown in figure 3. We begin by estimating approximation errors in force computations arising from the use of cluster summation rules, and subsequently estimate approximation errors in energy computation. The approximate force on any representative atom  $K \in \mathcal{L}_h$  is given by

$$\tilde{f}_K^h = -2 \sum_{J \in \mathcal{L}_h} n_J \sum_{k \in C_J} g(k) \Phi^h(X_k | X_K), \quad (14a)$$

$$g(k) = \sum_{\substack{j \in \mathcal{L} \\ j \neq k}} \bar{K}'(|x_k - x_j|) \frac{x_k - x_j}{|x_k - x_j|}. \quad (14b)$$

where  $\mathcal{L}_h \subset \mathcal{L}$  is a collection of representative atoms in the chain,  $C_J$  denotes the set of atoms located in the cluster centered at representative atom  $J$  with a cluster weight of  $n_J$ . Cluster weights are computed such that shape-functions of the finite-element triangulation of representative atoms are summed exactly (Knap & Ortiz, 2001).  $\Phi^h(X_k|X_K)$  denotes the value of the shape-function associated with representative atom  $K$  evaluated at atom  $k$ . We further note that  $\bar{K}'(|x_k - x_j|)$  decays as  $\frac{1}{|x_k - x_j|^{p+1}}$  (up to a constant factor) from assumption A1.

We first estimate  $g(k)$  before computing an estimate for the approximate force in equation (14). To this end we note the following bounds of the  $p$ -series which appear repeatedly in the estimates to follow:

$$S(k; p) = \sum_{t=k+1}^{\infty} \frac{1}{t^p} \geq \int_{k+1}^{\infty} \frac{dy}{y^p} = \frac{1}{(p-1)(k+1)^{p-1}} \quad k > 1, \quad (15a)$$

$$S(k; p) = \sum_{t=k+1}^{\infty} \frac{1}{t^p} \leq \int_k^{\infty} \frac{dy}{y^p} = \frac{1}{(p-1)k^{p-1}} \quad k > 1. \quad (15b)$$

The lower bound and the upper bound will approach each other for large  $k$ . In the computation of error estimates below, for  $k > r_{th2}$  (a threshold distance) we will approximate the  $p$ -series with their upper bound

$$S(k; p) = \frac{1}{(p-1)k^{p-1}} + O\left(\frac{1}{k^p}\right). \quad (16)$$

We define  $r' = \max\{r_{th}, r_{th2}\}$  and assume  $r_0 \gg r'$  for simplicity. We now proceed to estimate the force  $g(k)$  on atom  $k$ . For  $k \geq r'$ , using symmetry and assumption A1

$$\begin{aligned} g(k) &= \sum_{t=k+1}^{\infty} \left\{ \frac{1}{(ta_1)^{p+1}} - \frac{1}{(ka_1 + (t-k)a_2)^{p+1}} \right\} \\ &= \sum_{t=k+1}^{\infty} \frac{1}{t^{p+1}} \left\{ \frac{1}{a_1^{p+1}} - \frac{1}{((a_1 - a_2)\frac{k}{t} + a_2)^{p+1}} \right\} \\ &= \sum_{t=k+1}^{\infty} \frac{1}{t^{p+1}} \left( \frac{1}{a_1^{p+1}} - \frac{1}{a_2^{p+1}} \left\{ 1 + (p+1)\frac{a_2 - a_1}{a_2} \frac{k}{t} + O\left(\left(\frac{a_2 - a_1}{a_2}\right)^2\right) \right\} \right) \\ &= \frac{(p+1)(a_2 - a_1)}{a_2^{p+2}} \left\{ S(k; p+1) - kS(k; p+2) \right\} + O\left(\frac{1}{a_2^{p+1}} \left(\frac{a_2 - a_1}{a_2}\right)^2\right) \\ &\qquad\qquad\qquad \frac{(a_2 - a_1)}{a_2} \ll 1 \quad \text{from A2} \\ &\approx \frac{\alpha}{k^p} \quad \text{where } \alpha = \frac{a_2 - a_1}{pa_2^{p+2}} \quad \text{from equation (16)}. \quad (17) \end{aligned}$$

Similarly we obtain for  $k \leq -r'$ ,

$$g(k) \approx \frac{\alpha}{|k|^p}. \quad (18)$$

Now we estimate the approximate force on the representative atom  $K = 0$  using cluster summation rules. Using equations (14), (17)-(18) we get

$$\begin{aligned}
 -\frac{\tilde{f}_0^h}{2} &= n_0 \sum_{k=0}^{r'} g(k) \left(1 - \frac{k}{Ny}\right) + n_0 \sum_{k=1}^{r'} g(-k) \left(1 - \frac{k}{N}\right) + \alpha n_0 \sum_{k=r'+1}^{r_0} \frac{1 - \frac{k}{Ny}}{k^p} \\
 &\quad + \alpha n_0 \sum_{k=r'+1}^{r_0} \frac{1 - \frac{k}{N}}{k^p} + \alpha n_{-N} \sum_{k=N-r_0}^N \frac{1 - \frac{k}{N}}{k^p} + \alpha n_{Ny} \sum_{k=Ny-r_0}^{Ny} \frac{1 - \frac{k}{Ny}}{k^p} \\
 &= n_0 \sum_{k=-r'}^{r'} g(k) + \frac{2\alpha n_0}{p-1} \left( \frac{1}{(r'+1)^{p-1}} - \frac{1}{r_0^{p-1}} \right) + O\left(\frac{\alpha n_0}{N}\right) \quad (\text{for } N \gg r_0 \gg 1 \text{ by A3}).
 \end{aligned} \tag{19}$$

Using the same approach, the exact force (without cluster summation rules) on the representative atom  $K = 0$  is computed to be

$$-\frac{f_0^h}{2} = \sum_{k=-r'}^{r'} g(k) + \frac{2\alpha}{(p-1)(r'+1)^{p-1}} + O\left(\frac{\alpha}{N}\right). \tag{20}$$

Thus an estimate for the error in the force calculation using node-based cluster rules is given by

$$f_0^h - \tilde{f}_0^h \approx 2(n_0 - 1) \left\{ \sum_{k=-r'}^{r'} g(k) + \frac{2\alpha}{(p-1)(r'+1)^{p-1}} \right\} - \frac{4\alpha n_0}{(p-1)r_0^{p-1}}. \tag{21}$$

We now discuss some attributes of the error estimate in equation (21). Firstly, we note that the error will vanish if  $F_1 = F_2$ , as in this case  $\alpha = 0$  and  $g(k) = 0 \forall k$ . But if  $F_1 \neq F_2$ , then the absolute error in the force scales linearly with the element size and results in a relative error in the displacements that is  $O(1)$ . This follows from the fact that  $n_0$  scales as  $\frac{N(1+y)}{4r_0}$  for  $N \gg r_0 \gg 1$ . This observation was first made in [Luskin & Ortner \(2009\)](#) using nearest neighbor interatomic interactions. The reason for this uncontrolled error is that forces on atoms drop rapidly away from the element boundary. But the cluster weights are computed such that shape-functions are summed exactly, which is a suitable quadrature rule if the forces are distributed evenly, but results in highly inaccurate forces otherwise.

We now turn to the computation of error estimates when node-based cluster summation rules are employed on lattice sums appearing in the evaluation of the energy of a system. We first compute the exact energy of atoms in elements  $BA$  and  $AC$ . We denote by  $\varepsilon_1$  and  $\varepsilon_2$  the energy per atom in an infinite chain with interatomic spacings  $a_1$  and  $a_2$  respectively. The exact energy is then given by

$$\begin{aligned}
 E &= \sum_{k=0}^{Ny} \varepsilon(k) + \sum_{k=1}^N \varepsilon(-k) \\
 &= \sum_{k=0}^{Ny} \Delta\varepsilon(k) + \sum_{k=1}^N \Delta\varepsilon(-k) + Ny\varepsilon_1 + N\varepsilon_2,
 \end{aligned} \tag{22}$$

where  $\varepsilon(k)$  is the energy of atom  $k$  in the environment of its neighbors, and  $\Delta\varepsilon(k) = \varepsilon(k) - \varepsilon_1$  for  $k \geq 0$ ,  $\Delta\varepsilon(-k) = \varepsilon(-k) - \varepsilon_2$  for  $k > 0$ . We now compute  $\Delta\varepsilon(k)$  and  $\Delta\varepsilon(-k)$  for  $k > r'$ . Following on similar lines as our estimate in equations (17)-(18),

$$\begin{aligned}
 \Delta\varepsilon(k) &= \sum_{t=k+1}^{\infty} \frac{1}{(ka_1 + (t-k)a_2)^p} - \frac{1}{(ta_1)^p} = \sum_{t=k+1}^{\infty} \frac{1}{t^p} \left\{ \frac{1}{(a_2 + \frac{k}{t}(a_1 - a_2))^p} - \frac{1}{a_1^p} \right\} \\
 &\approx \frac{a_1 - a_2}{(p-1)a_2^{p+1}} \frac{1}{k^{p-1}},
 \end{aligned} \tag{23}$$

$$\Delta\varepsilon(-k) \approx \frac{a_2 - a_1}{(p-1)a_2^{p+1}} \frac{1}{k^{p-1}} \approx -\Delta\varepsilon(k). \tag{24}$$

The energy of atoms in elements  $BA$  and  $AC$  can now be estimated using equations (23)-(24) as

$$\begin{aligned}
 E &= (Ny)\varepsilon_1 + N\varepsilon_2 + \sum_{k=-r'}^{r'} \Delta\varepsilon(k) + \sum_{k=r'+1}^N \Delta\varepsilon(-k) + \sum_{k=r'+1}^{Ny} \Delta\varepsilon(k) \\
 &\approx (Ny)\varepsilon_1 + N\varepsilon_2 + \sum_{k=-r'}^{r'} \Delta\varepsilon(k) + \sum_{k=N+1}^{Ny} \Delta\varepsilon(k) \quad (\text{from equation (24)}) \\
 &\approx (Ny)\varepsilon_1 + N\varepsilon_2 + \sum_{k=-r'}^{r'} \Delta\varepsilon(k) + \beta \left( \frac{1}{(N+1)^{p-2}} - \frac{1}{(Ny)^{p-2}} \right) \quad (\text{from equation (16)}) \\
 &= (Ny)\varepsilon_1 + N\varepsilon_2 + \sum_{k=-r'}^{r'} \Delta\varepsilon(k) + O\left(\frac{\beta}{N^{p-2}}\right).
 \end{aligned} \tag{25}$$

where  $\beta = \frac{a_1 - a_2}{(p-1)(p-2)a_2^{p+1}}$ . We now proceed to estimate the energy computed using node-based cluster summation rules. The expression for energy of the system upon using cluster summation rules for the lattice sums is given by

$$\tilde{E} = \sum_{J \in \mathcal{L}_h} n_J \sum_{k \in \mathcal{C}_J} \varepsilon(k), \tag{26}$$

where  $\varepsilon(k) = \sum_{\substack{j \in \mathcal{L} \\ j \neq k}} K(|x_k - x_j|)$ . In the present analysis of 1D mono-atomic chain with three representative atoms, this reduces to

$$\begin{aligned}
\tilde{E} &= (n_{-N} + n_0)\varepsilon_2 r_0 + (n_{Ny} + n_0)\varepsilon_1 r_0 + n_0 \sum_{k=-r_0}^{r_0} \Delta\varepsilon(k) \\
&\quad + n_{-N} \sum_{k=N-r_0}^N \Delta\varepsilon(-k) + n_{Ny} \sum_{k=Ny-r_0}^{Ny} \Delta\varepsilon(k) \\
&= (n_{-N} + n_0)\varepsilon_2 r_0 + (n_{Ny} + n_0)\varepsilon_1 r_0 + n_0 \left( \sum_{k=-r_0}^{-r'-1} \Delta\varepsilon(k) + \sum_{k=-r'}^{r'} \Delta\varepsilon(k) + \sum_{k=r'+1}^{r_0} \Delta\varepsilon(k) \right) + O\left(\frac{\beta n_0}{N^{p-2}}\right) \\
&\approx (n_{-N} + n_0)\varepsilon_2 r_0 + (n_{Ny} + n_0)\varepsilon_1 r_0 + n_0 \sum_{k=-r'}^{r'} \Delta\varepsilon(k) \quad (\text{as } \Delta\varepsilon(k) = -\Delta\varepsilon(-k) \text{ for } k > r').
\end{aligned} \tag{27}$$

We note that for  $N \gg r_0 \gg 1$ , the expressions for cluster weights, computed by enforcing that shape-functions are summed exactly, reduce to

$$n_{-N} \approx \frac{N}{2r_0}, \quad n_0 \approx \frac{N(1+y)}{4r_0}, \quad n_{Ny} \approx \frac{Ny}{2r_0}. \tag{28}$$

Using equations (25)-(28), we estimate the approximation error in the energy evaluation using node-based cluster rules to be

$$\tilde{E} - E \approx \frac{N(y-1)}{4}(\varepsilon_2 - \varepsilon_1) + (n_0 - 1) \sum_{k=-r'}^{r'} \Delta\varepsilon(k). \tag{29}$$

The relative error in the energy computation is given by

$$\frac{|\tilde{E} - E|}{E} \approx \left| \frac{(y-1)}{4(y+1)\varepsilon_1}(\varepsilon_2 - \varepsilon_1) + \frac{1}{4r_0\varepsilon_1} \sum_{k=-r'}^{r'} \Delta\varepsilon(k) \right|. \tag{30}$$

From the above estimates it is evident that the error in energy evaluation upon using node-based cluster summation rules vanishes when  $F_1 = F_2$ , as in this case  $\varepsilon_1 = \varepsilon_2$  and  $\Delta\varepsilon(k) = 0$  for  $k \in \mathcal{L}$ . However, if  $F_1 \neq F_2$ , the absolute error in energy scales linearly with the element size, similar to the approximation error in force evaluation given by equation (21). The relative error, from equation (30), is  $O(F_1 - F_2)$  and is first order accurate. We remark that the errors in energy while using node-based cluster rules are larger than the corresponding errors incurred by using element-based cluster rules that are analyzed subsequently in section 3.3.

### 3.2 Node-based cluster rules on energy

The non-conservative nature of approximate forces in the formulation proposed in [Knap & Ortiz \(2001\)](#) is a result of employing cluster summation rules directly on forces as opposed to

computing the forces as tangents of an approximate energy. To resolve this deficiency in the formulation, [Eidel & Stukowski \(2009\)](#) have proposed to introduce cluster summation rules only on the energy of a system (equation (26)) and compute the forces as tangents of this approximate energy. The approximation error in the energy has been computed in section 3.1 and is given by equation (29). We now estimate the approximation error in the force computation for this formulation. Using the notation introduced in section 3.1, the approximate force on a representative atom  $K$  is given by

$$\tilde{f}_K^h = \sum_{J \in \mathcal{L}_h} n_J \sum_{k \in C_J} \left( \sum_{\substack{j \in \mathcal{L} \\ j \neq k}} f_{kj} \Phi^h(X_j | X_K) - \Phi^h(X_k | X_K) \sum_{\substack{j \in \mathcal{L} \\ j \neq k}} f_{kj} \right), \quad (31a)$$

$$f_{kj} = \bar{K}'(|x_k - x_j|) \frac{x_k - x_j}{|x_k - x_j|}. \quad (31b)$$

We will restrict our analysis to the special case of  $F_1 = F_2$ , which, as will be demonstrated, produces the leading order error for this formulation. We note that the second term in the above expression vanishes as  $\sum_{\substack{j \in \mathcal{L} \\ j \neq k}} f_{kj} = 0$  for affine deformations. The non-zero contribution to the approximate force, which is also the approximation error as the exact force is zero, comes from the first term in the expression. We denote  $g(k) = \sum_{\substack{j \in \mathcal{L} \\ j \neq k}} f_{kj} \Phi^h(X_j | X_0)$  and estimate  $g(k)$  for  $\{-r_0, \dots, r_0\}$ . We remark that the value of  $g(k)$  for  $k \in \{-N, \dots, -N + r_0\} \cup \{Ny - r_0, \dots, Ny\}$  is small compared to the value of  $g(k)$  for  $k \in \{-r_0, \dots, r_0\}$ , and can be neglected as it will only result in a relative error of  $O(\frac{1}{N})$  as seen in section 3.1. For the central potential we are considering in this analysis ( $\bar{K}(|x_i - x_j|)$ ), the expression for  $g(k)$ ,  $k \in \{-r_0, \dots, r_0\}$ , is given by

$$\begin{aligned} g(k) &= \sum_{j=k+1}^{Ny} \bar{K}'(a_1|j-k|) \frac{Ny-j}{Ny} - \left\{ \sum_{j=0}^{k-1} \bar{K}'(a_1|j-k|) \frac{Ny-j}{Ny} + \sum_{j=1}^N \bar{K}'(a_1|j+k|) \frac{N-j}{N} \right\} \quad k > 0, \\ g(-k) &= - \sum_{j=k+1}^N \bar{K}'(a_1|j-k|) \frac{N-j}{N} + \left\{ \sum_{j=0}^{k-1} \bar{K}'(a_1|j-k|) \frac{N-j}{N} + \sum_{j=1}^{Ny} \bar{K}'(a_1|j+k|) \frac{Ny-j}{Ny} \right\} \quad k > 0, \\ g(0) &= \sum_{j=1}^{Ny} \bar{K}'(a_1j) \frac{Ny-j}{Ny} - \sum_{j=1}^N \bar{K}'(a_1j) \frac{N-j}{N}. \end{aligned} \quad (32)$$

For brevity, we further define  $s(k) = g(k) + g(-k)$  for  $k = 0, 1, \dots, r_0$ . Upon rearranging, we obtain

$$\begin{aligned} s(k) &= \sum_{j=N}^{Ny} \left( \bar{K}'(a_1|j-k|) + \bar{K}'(a_1|j+k|) \right) \left( 1 - \frac{j}{Ny} \right) + \left( \frac{1}{N} - \frac{1}{Ny} \right) z(k), \quad \text{where} \\ z(k) &= \sum_{j=k+1}^N \bar{K}'(a_1|j-k|)j - \sum_{j=0}^{k-1} \bar{K}'(a_1|j-k|)j + \sum_{j=1}^N \bar{K}'(a_1|j+k|)j \quad \text{for } k = 1 \dots r_0 \\ z(0) &= 2 \sum_{j=1}^N \bar{K}'(a_1j)j. \end{aligned} \quad (33)$$

Noting  $N \gg r_0$ , and using the decay for central potential in assumption A1 along with the properties of p-series (equation 16), the first term in  $s(k)$  is  $O(\frac{1}{N^p})$  which is higher order compared to the second term and we drop it for simplicity. Thus,  $s(k) \approx (\frac{1}{N} - \frac{1}{Ny})z(k)$ . Finally, the approximation error in the computation of force on representative atom  $K = 0$  can now be expressed as

$$\begin{aligned} \tilde{f}_0^h - f_0^h &= \tilde{f}_0^h \approx n_0 \left( \frac{1}{N} - \frac{1}{Ny} \right) \left\{ \frac{1}{2}z(0) + \sum_{k=1}^{r_0} z(k) \right\} \\ &= \frac{(1+y)}{4r_0} \left( 1 - \frac{1}{y} \right) \left\{ \frac{1}{2}z(0) + \sum_{k=1}^{r_0} z(k) \right\}. \end{aligned} \quad (34)$$

We remark that  $z(k)$  is  $O(1)$  for  $k = 0, 1 \dots r_0$ , with the exception of  $z(0) \approx 0$  near ground-state, and from equation (34) it is evident that  $\tilde{f}_0^h \neq 0$  for  $y \neq 1$ . Thus, the patch test fails for any coarse-graining, and the formulation is only consistent with uniform meshes which are never used in the quasi-continuum method. Further, with increasing  $y$  the force increases and can become uncontrollably large for rapid rates of coarse-graining. Implications of this inconsistent formulation for various kinds of meshes were analyzed in [Luskin & Ortner \(2009\)](#) using nearest neighbor harmonic interactions, where, in some cases of graded or non-smooth meshes, large relative errors independent of mesh size were observed. Due to the failure of patch test, a systematic convergence of the scheme is not guaranteed which is also confirmed from numerical simulations in section 6.

### 3.3 Element-based cluster rules

As opposed to introducing clusters at nodes of the triangulation, we consider clusters that are introduced in the interior of elements, preferably at the Gauss points, following quadrature rules in numerical approximation schemes. Figure 4 illustrates this scenario where one cluster is introduced inside each element. We define  $k_1(i) = \frac{Ny}{2} - i$ , and  $k_2(i) = \frac{N}{2} - i$ , which for  $i = -r_0 \dots r_0$  denote the positions of the atoms in the clusters located in the two elements. We assume without loss of generality that  $\frac{N}{2}$  and  $\frac{Ny}{2}$  are integers. Using the notation introduced in section 3.1, the approximate energy is given by

$$\begin{aligned} \tilde{E} &= n_1 \sum_{i=-r_0}^{r_0} \varepsilon(k_1(i)) + n_2 \sum_{i=-r_0}^{r_0} \varepsilon(-k_2(i)) \\ &= n_1(2r_0 + 1)\varepsilon_1 + n_2(2r_0 + 1)\varepsilon_2 + n_1 \sum_{i=-r_0}^{r_0} \Delta\varepsilon(k_1(i)) + n_2 \sum_{i=-r_0}^{r_0} \Delta\varepsilon(-k_2(i)) \end{aligned} \quad (35)$$

In the above expression,  $n_1$  and  $n_2$  are weights of the clusters located inside elements  $AC$  and  $BA$  respectively, and are computed such that piecewise constant functions are summed exactly—a zeroth order quadrature rule. Thus, we obtain  $n_1 = \frac{Ny}{2r_0+1}$  and  $n_2 =$

$\frac{N}{2r_0+1}$ . In fact, since the clusters are centered at mid-points of the elements, which are the Gauss quadrature points, the cluster rule is first order accurate. Using a similar analysis as adopted in section 3.1, we note that  $\sum_{i=-r_0}^{r_0} \Delta\varepsilon(k_1(i)) = O(\frac{1}{(Ny)^{p-1}})$  and  $\sum_{i=-r_0}^{r_0} \Delta\varepsilon(-k_2(i)) = O(\frac{1}{(N)^{p-1}})$ , which are higher order terms. Thus,  $\tilde{E} \approx N\varepsilon_2 + Ny\varepsilon_1$ . Using equation (25), the approximation error in energy using an element-based cluster rule is estimated as

$$\tilde{E} - E \approx - \sum_{k=-r'}^{r'} \Delta\varepsilon(k). \quad (36)$$

The corresponding relative error in the energy is given by

$$\frac{|\tilde{E} - E|}{E} \approx \left| \frac{1}{N(1+y)\epsilon_1} \sum_{k=-r'}^{r'} \Delta\varepsilon(k) \right|. \quad (37)$$

Comparing equations (36) and (37) with equations (29) and (30), it is evident that the approximation errors in energy in using element-based cluster rules are smaller compared to the errors incurred by using node-based cluster rules. We now compute the error in forces, which are computed as tangents of the approximate energy. Element-based cluster rules too fail the patch test as will be demonstrated from the estimate below. Considering the case  $F_1 = F_2$  and following on similar lines as in section 3.2, the approximation error in the force on representative atom  $K = 0$  is estimated as

$$\begin{aligned} \tilde{f}_0^h &= \sum_{i=-r_0}^{r_0} \frac{1}{2r_0+1} \left( z(k_1(i)) - z(k_2(i)) + N \sum_{j=1}^{Ny} \bar{K}'(a_1|j+k_2(i)|) - Ny \sum_{j=1}^N \bar{K}'(a_1|j+k_1(i)|) \right), \\ z(k_1(i)) &= \sum_{j=0}^{k_1(i)-1} \bar{K}'(a_1|j-k_1(i)|)j - \sum_{j=k_1(i)+1}^{Ny} \bar{K}'(a_1|j-k_1(i)|)j + y \sum_{j=1}^N \bar{K}'(a_1|j+k_1(i)|)j, \\ z(k_2(i)) &= \sum_{j=0}^{k_2(i)-1} \bar{K}'(a_1|j-k_2(i)|)j - \sum_{j=k_2(i)+1}^N \bar{K}'(a_1|j-k_2(i)|)j + \frac{1}{y} \sum_{j=1}^{Ny} \bar{K}'(a_1|j+k_2(i)|)j. \end{aligned} \quad (38)$$

We remark that  $\tilde{f}_0^h \neq 0$  for  $y \neq 1$ , and  $\tilde{f}_0^h = O(\frac{y-1}{N^{p-1}})$ . We refer to the appendix for further details on this estimate. Thus, for any general coarse-graining, the element-based cluster rules also fail the patch test. However, we note that this error is smaller than the error in node-based cluster rules (cf. equation (34)) as it scales inversely with the element size for large elements. We note that this inverse scaling of the error with element size is only true for  $N \gg r_0 \gg 1$ , which is not valid in the transition region—between fully coarse-grained (large) elements to atomic scale (small) elements—where  $N > 2r_0$ , but  $N \sim 2r_0$ , and this case needs to be further investigated.

The primary cause for the failure of patch test, which is a necessary condition for the convergence of numerical approximations, is that cluster rules which are introduced in the spirit of numerical quadratures are not compatible with non-local representations of energies. This aspect has also been highlighted in section 2. The notion of numerical

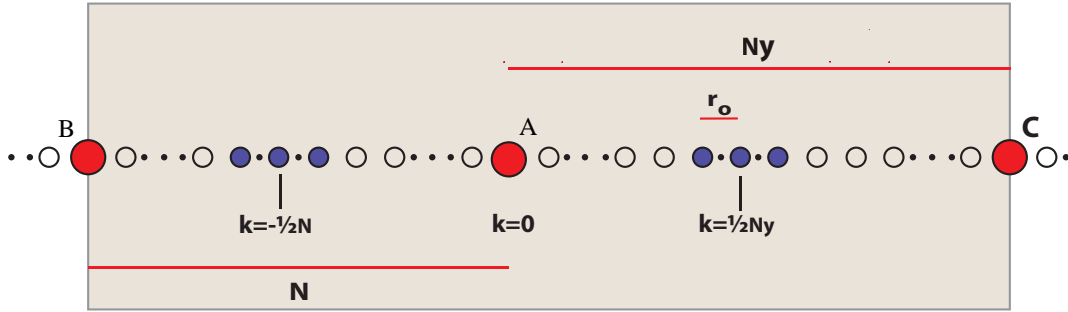


Fig. 4. Schematic demonstrating element-based cluster rules: circles in red denote representative atoms while circles in blue denote atoms lying within clusters; clusters are located at the center of elements.

quadratures has been developed for local functions, and its use on non-local representations of energies appears incompatible—at least in the sense of satisfying the patch test. We rectify this problem by first reformulating the extended interactions in interatomic potentials into a local form, and subsequently introduce the quasi-continuum reduction.

#### 4 Local reformulation of interatomic potentials

The energy of a single-component material system described by interatomic potentials, using the notation introduced in section 2, is given by

$$E(\mathbf{q}) = \sum_{i \in \mathcal{L}} \varepsilon_i(\mathbf{q}), \quad (39)$$

$$\varepsilon_i(\mathbf{q}) = \sum_{j \in \mathcal{L}, j \neq i} \bar{K}(|\mathbf{x}_i - \mathbf{x}_j|), \quad (40)$$

where  $\varepsilon_i(\mathbf{q})$  denotes the energy of atom  $i$  in the environment of its neighbors, and  $\bar{K}$  denotes the kernel representing extended interatomic interactions. The widely used interatomic potentials include Lennard Jones potential, Morse potential, and embedded atom method (EAM) potentials (cf. e. g., [Lennard-Jones \(1924\)](#); [Morse \(1929\)](#); [Daw & Baskes \(1984\)](#); [Johnson \(1988\)](#); [Sutton & Chen \(1990\)](#)). The kernels used in these interatomic potentials are mostly either the *exponential kernel* ( $e^{-\alpha|\mathbf{x}_i - \mathbf{x}_j|}$ ), or kernels of the form  $\frac{1}{|\mathbf{x}_i - \mathbf{x}_j|^m}$ , where  $m$  is a positive integer, which we refer to in this article by *Lennard-Jones kernels*. We present the local reformulations of these kernels, which convert the extended interactions often represented in a non-local form into a local variational problem. We first consider the case of exponential kernels, and then discuss our approach for Lennard-Jones kernels.

### 4.1 Exponential kernels

We consider the Morse potential which uses an exponential kernel to demonstrate our ideas. The energy of a single component material system in this case has the following form

$$\begin{aligned}
 E^M(\mathbf{q}) &= \sum_{\mathbf{i} \in \mathcal{L}} \varepsilon_{\mathbf{i}}^M(\mathbf{q}), \\
 \varepsilon_{\mathbf{i}}^M(\mathbf{q}) &= \frac{V_e}{2} \sum_{\mathbf{j} \in \mathcal{L}, \mathbf{j} \neq \mathbf{i}} \left\{ (1 - e^{-\alpha(|\mathbf{x}_{\mathbf{i}} - \mathbf{x}_{\mathbf{j}}| - x_e)})^2 - 1 \right\} \\
 &= \frac{V_e}{2} \sum_{\mathbf{j} \in \mathcal{L}, \mathbf{j} \neq \mathbf{i}} \left\{ -2C e^{-\alpha|\mathbf{x}_{\mathbf{i}} - \mathbf{x}_{\mathbf{j}}|} + C^2 e^{-2\alpha|\mathbf{x}_{\mathbf{i}} - \mathbf{x}_{\mathbf{j}}|} \right\} \quad C = e^{\alpha x_e}, \quad (41)
 \end{aligned}$$

where  $\alpha$ ,  $x_e$  and  $V_e$  are material constants. In order to construct a local reformulation of this non-local representation, we represent the atoms by regularized dirac distributions denoted by  $\delta(\mathbf{y} - \mathbf{x}_{\mathbf{i}})$  for  $\mathbf{i} \in \mathcal{L}$ . Further, we define  $b(\mathbf{y}; \mathbf{q}) = \sum_{\mathbf{i} \in \mathcal{L}} \delta(\mathbf{y} - \mathbf{x}_{\mathbf{i}})$ . The energy of the system can now be represented as

$$\begin{aligned}
 E^M(\mathbf{q}) &= -V_e C \int_{\Omega_0} \int_{\Omega_0} b(\mathbf{y}; \mathbf{q}) e^{-\alpha|\mathbf{y} - \mathbf{y}'|} b(\mathbf{y}'; \mathbf{q}) d\mathbf{y} d\mathbf{y}' \\
 &\quad + \frac{V_e C^2}{2} \int_{\Omega_0} \int_{\Omega_0} b(\mathbf{y}; \mathbf{q}) e^{-2\alpha|\mathbf{y} - \mathbf{y}'|} b(\mathbf{y}'; \mathbf{q}) d\mathbf{y} d\mathbf{y}'. \quad (42)
 \end{aligned}$$

In the above expression,  $\Omega_0 \subset \mathbb{R}^3$  is a simply connected bounded open set that contains the compact support of  $b$  (the region where  $b$  is non-zero). We note that the right-hand sides of equation (41) and equation (42) differ by the self-energy of the atoms which is an inconsequential constant that does not change the ground-state solution. This self energy is explicitly computed and subtracted in numerical computations. We further remark that the atoms, which are dirac distributions in a field formulation, are approximated in equation (42) by regularized dirac distributions to avoid infinite self energies if the Kernel corresponding to the non-local interatomic interactions is singular. This introduces an approximation in the energy of the system, which, however, can be made arbitrarily close to the exact energy by considering the regularization to be arbitrarily close to the dirac distribution.

We define  $\phi_1(\mathbf{y}; \mathbf{q}) = \int e^{-\alpha|\mathbf{y} - \mathbf{y}'|} b(\mathbf{y}'; \mathbf{q}) d\mathbf{y}'$  and take the Fourier transform of this equation to get

$$\frac{(\alpha^2 + |\mathbf{k}|^2)^2}{8\pi\alpha} \hat{\phi}_1(\mathbf{k}) = \hat{b}(\mathbf{k}), \quad (43)$$

where  $\frac{8\pi\alpha}{(\alpha^2 + |\mathbf{k}|^2)^2}$  is the Fourier transform of  $e^{-\alpha|\mathbf{y}|}$ . Taking the inverse Fourier transform of equation (43) we arrive at

$$\frac{1}{8\pi\alpha} \left\{ \nabla^4 - 2\alpha^2 \nabla^2 + \alpha^4 \right\} \phi_1(\mathbf{y}; \mathbf{q}) = b(\mathbf{y}; \mathbf{q}). \quad (44)$$

In effect we have constructed the partial differential equation whose Green's function is the exponential kernel. Rewriting equation (44) in a variational form we arrive at

$$I_1(\mathbf{q}) = \inf_{\varphi_1 \in H_0^2(\mathbb{R}^3)} \frac{1}{8\pi\alpha} \left\{ \frac{1}{2} \int_{\Omega} (\nabla^2 \varphi_1)^2 d\mathbf{y} + \alpha^2 \int_{\Omega} |\nabla \varphi_1|^2 d\mathbf{y} + \frac{\alpha^4}{2} \int_{\Omega} \varphi_1^2 d\mathbf{y} - 8\pi\alpha \int_{\Omega} b(\mathbf{q}) \varphi_1 d\mathbf{y} \right\}. \quad (45)$$

In practice, the function space in this variational problem is chosen to be  $H_0^2(\Omega)$ , where  $\Omega \subset \mathbb{R}^3$  denotes the compact support of  $\varphi_1$  and other potentials we subsequently compute. For a sufficiently fast decay of these potentials away from the positions of atoms in the crystallite, this is a reasonable approximation when  $\mathcal{L} \subset\subset \Omega$  and we will work under this approximation in the remainder of the formulation. We also remark that the variation problem in equation (45) is well-posed and a minimizer exists which is unique. This follows from the convexity, lower semi-continuity, and coercivity of the energy functional (cf. [Dacorogna \(1989\)](#)). Therefore, in the subsequent expressions we will replace  $\inf$  with  $\min$ . The solution of the partial differential in equation (44) is now given by  $\phi_1 = \arg \min I_1$ .

The variational problem in equation (45) requires the trial functions to be in  $H_0^2(\Omega)$ , and commonly used basis functions in numerical schemes like  $C^0$  finite-elements are not contained in this function space. To this end, we consider the equivalent mixed variational formulation given by

$$I_1(\mathbf{q}) = \min_{\varphi_1 \in H_0^1(\Omega)} \max_{\varrho_1 \in H_0^1(\Omega)} \frac{1}{8\pi\alpha} \left\{ \alpha^2 \int_{\Omega} |\nabla \varphi_1|^2 d\mathbf{y} + \frac{\alpha^4}{2} \int_{\Omega} \varphi_1^2 d\mathbf{y} - 8\pi\alpha \int_{\Omega} b(\mathbf{q}) \varphi_1 d\mathbf{y} - \int_{\Omega} \nabla \varphi_1 \cdot \nabla \varrho_1 d\mathbf{y} - \frac{1}{2} \int_{\Omega} \varrho_1^2 d\mathbf{y} \right\}. \quad (46)$$

The corresponding Euler-Lagrange equations are

$$\nabla^2 \rho_1(\mathbf{y}; \mathbf{q}) - 2\alpha^2 \nabla^2 \phi_1(\mathbf{y}; \mathbf{q}) + \alpha^4 \phi_1(\mathbf{y}; \mathbf{q}) - 8\pi\alpha b(\mathbf{y}; \mathbf{q}) = 0, \quad (47a)$$

$$\nabla^2 \phi_1(\mathbf{y}; \mathbf{q}) - \rho_1(\mathbf{y}; \mathbf{q}) = 0. \quad (47b)$$

which is a system of partial differential equations equivalent to the partial differential equation in equation (44). In the above equation  $\phi_1$  and  $\rho_1$  denote the minimizer and maximizer of the mixed variational formulation in equation (46) respectively. We note that the order of minimization and maximization can be interchanged in equation (46), which follows from the existence of saddle-point for the convex-concave functional (cf. e. g. [Boyd & Vandenberghe \(2004\)](#)).

Following on similar lines we define  $\phi_2(\mathbf{y}; \mathbf{q}) = \int e^{-2\alpha|\mathbf{y}-\mathbf{y}'|} b(\mathbf{y}'; \mathbf{q}) d\mathbf{y}'$ , and the corre-

sponding mixed variational problem for  $\phi_2$  is given by

$$I_2(\mathbf{q}) = \min_{\varphi_2 \in H_0^1(\Omega)} \max_{\varrho_2 \in H_0^1(\Omega)} \frac{1}{16\pi\alpha} \left\{ 4\alpha^2 \int_{\Omega} |\nabla\varphi_2|^2 d\mathbf{y} + 8\alpha^4 \int_{\Omega} \varphi_2^2 d\mathbf{y} - 16\pi\alpha \int_{\Omega} b(\mathbf{q})\varphi_2 d\mathbf{y} - \int_{\Omega} \nabla\varphi_2 \cdot \nabla\varrho_2 d\mathbf{y} - \frac{1}{2} \int_{\Omega} \varrho_2^2 d\mathbf{y} \right\}, \quad (48)$$

where  $\phi_2$  is the minimizer of the above mixed variational problem. Using the Euler-Lagrange equations corresponding to the mixed variational problems in equations (46) and (48), we note that

$$I_1(\mathbf{q}) = -\frac{1}{2} \int_{\Omega} b(\mathbf{y}; \mathbf{q})\phi_1(\mathbf{y}; \mathbf{q})d\mathbf{y}, \quad I_2(\mathbf{q}) = -\frac{1}{2} \int_{\Omega} b(\mathbf{y}; \mathbf{q})\phi_2(\mathbf{y}; \mathbf{q})d\mathbf{y}. \quad (49)$$

Using equations (42) and (49), we can rewrite the energy of the system as

$$E^M(\mathbf{q}) = 2CV_e I_1(\mathbf{q}) - C^2V_e I_2(\mathbf{q}). \quad (50)$$

Using equations (45)-(50) we arrive at the following saddle-point problem:

$$E^M(\mathbf{q}) = \min_{\substack{\varphi_1 \in H_0^1(\Omega) \\ \varrho_2 \in H_0^1(\Omega)}} \max_{\substack{\varphi_2 \in H_0^1(\Omega) \\ \varrho_1 \in H_0^1(\Omega)}} \int_{\Omega} L(\varphi_1, \varrho_1, \varphi_2, \varrho_2; \mathbf{q})d\mathbf{y},$$

$$L(\varphi_1, \varrho_1, \varphi_2, \varrho_2; \mathbf{q}) = \frac{2CV_e}{8\pi\alpha} \left\{ \alpha^2 |\nabla\varphi_1|^2 + \frac{\alpha^4}{2} \varphi_1^2 - 8\pi\alpha b(\mathbf{q})\varphi_1 - \nabla\varphi_1 \cdot \nabla\varrho_1 - \frac{1}{2} \varrho_1^2 \right\} - \frac{C^2V_e}{16\pi\alpha} \left\{ 4\alpha^2 |\nabla\varphi_2|^2 + 8\alpha^4 \varphi_2^2 - 16\pi\alpha b(\mathbf{q})\varphi_2 - \nabla\varphi_2 \cdot \nabla\varrho_2 - \frac{1}{2} \varrho_2^2 \right\}. \quad (51)$$

The saddle-point problem in equation (51) is a local reformulation of the extended interactions with exponential kernels. The problem of computing ground-state properties of a system is then given by the variational problem

$$E_0^M = \min_{\mathbf{q} \in X} E^M(\mathbf{q}), \quad (52)$$

or equivalently the saddle-point problem on the Lagrangian  $L(\varphi_1, \varrho_1, \varphi_2, \varrho_2; \mathbf{q})$

$$E_0^M = \min_{\mathbf{q} \in X} \min_{\substack{\varphi_1 \in H_0^1(\Omega) \\ \varrho_2 \in H_0^1(\Omega)}} \max_{\substack{\varphi_2 \in H_0^1(\Omega) \\ \varrho_1 \in H_0^1(\Omega)}} \int_{\Omega} L(\varphi_1, \varrho_1, \varphi_2, \varrho_2; \mathbf{q})d\mathbf{y}. \quad (53)$$

The saddle-point problem in the above equation describes a crystallite in  $\mathbb{R}^3$  with finite number of atoms. Though we restrict our discussion of the formulation to a finite crystallite, the formulation itself and other remarks we made and will make subsequently are in general true for other systems like a periodic system, semi-infinite lattice, etc. For instance, a periodic system is realized by appropriately changing the function space in the formulation to  $H_{per}^1(Q)$ , where  $Q$  denotes the supercell, or  $H^1(Q)$  if the supercell is chosen such that  $\partial Q$  contains only planes of symmetry of the lattice.

We now consider the computation of forces on atoms, which corresponds to the outer minimization on  $\mathbf{q}$ . Consider the infinitesimal perturbation of atom positions given by a family of mappings  $\psi_\epsilon : \mathbb{R}^{3N_0} \rightarrow \mathbb{R}^{3N_0}$  with  $\epsilon \ll 1$  as the parameter. We denote by  $\psi_\epsilon^{\mathbf{i}} : \mathbb{R}^3 \rightarrow \mathbb{R}^3$  the infinitesimal perturbation of atom  $\mathbf{i}$  such that  $\psi_0^{\mathbf{i}} = id$  (identity mapping) and  $\frac{d}{d\epsilon}(\psi_\epsilon^{\mathbf{i}})_j \Big|_{\epsilon=0} = \Gamma_j^{\mathbf{i}}$  for  $\mathbf{i} \in \mathcal{L}$ ,  $j = 1, 2, 3$ .  $\Gamma^{\mathbf{i}}$  is often referred to as the generator of the infinitesimal mappings, and the directional derivative corresponding to this generator is given by

$$\begin{aligned}
 \frac{d}{d\epsilon} E^M(\psi_\epsilon(\mathbf{q})) \Big|_{\epsilon=0} &= \frac{d}{d\epsilon} \left( -2CV_e \int_{\Omega} b(\psi_\epsilon(\mathbf{q})) \phi_1 d\mathbf{y} + C^2 V_e \int_{\Omega} b(\psi_\epsilon(\mathbf{q})) \phi_2 d\mathbf{y} \right) \Big|_{\epsilon=0} \\
 &= 2CV_e \sum_{\mathbf{k} \in \mathcal{L}} \int_{\Omega} \frac{\partial \delta(\mathbf{y} - \psi_\epsilon^{\mathbf{k}}(\mathbf{x}_{\mathbf{k}}))}{\partial y_j} \frac{d(\psi_\epsilon^{\mathbf{k}})_j}{d\epsilon} \phi_1(\mathbf{y}) d\mathbf{y} \Big|_{\epsilon=0} \\
 &\quad - C^2 V_e \sum_{\mathbf{k} \in \mathcal{L}} \int_{\Omega} \frac{\partial \delta(\mathbf{y} - \psi_\epsilon^{\mathbf{k}}(\mathbf{x}_{\mathbf{k}}))}{\partial y_j} \frac{d(\psi_\epsilon^{\mathbf{k}})_j}{d\epsilon} \phi_2(\mathbf{y}) d\mathbf{y} \Big|_{\epsilon=0} \quad (\nabla_{\mathbf{r}} \delta(\mathbf{r} - \mathbf{r}') = -\nabla_{\mathbf{r}'} \delta(\mathbf{r} - \mathbf{r}')) \\
 &= -2CV_e \sum_{\mathbf{k} \in \mathcal{L}} \int_{\Omega} \delta(\mathbf{y} - \mathbf{x}_{\mathbf{k}}) \Gamma_j^{\mathbf{k}} \frac{\partial \phi_1(\mathbf{y})}{\partial y_j} d\mathbf{y} + C^2 V_e \sum_{\mathbf{k} \in \mathcal{L}} \int_{\Omega} \delta(\mathbf{y} - \mathbf{x}_{\mathbf{k}}) \Gamma_j^{\mathbf{k}} \frac{\partial \phi_2(\mathbf{y})}{\partial y_j} d\mathbf{y} \\
 &= - \sum_{\mathbf{k} \in \mathcal{L}} \left( 2CV_e \frac{\partial \phi_1}{\partial y_j}(\mathbf{x}_{\mathbf{k}}) - C^2 V_e \frac{\partial \phi_2}{\partial y_j}(\mathbf{x}_{\mathbf{k}}) \right) \Gamma_j^{\mathbf{k}}.
 \end{aligned} \tag{54}$$

The first equality in the above equation follows from the Euler Lagrange equations in  $\varphi_1, \varphi_2, \varrho_1, \varrho_2$ , or alternatively we refer to the Hellmann-Feynman theorem in a similar context (cf. chapter 3 in [Finnis \(2003\)](#)). We remark that the last equality in equation (54) is only approximately true as  $\delta(\mathbf{y} - \mathbf{x}_{\mathbf{k}})$  represents a regularized dirac distribution. As noted before, by considering the regularization to be arbitrarily close to the dirac distribution, the error in this approximation can be made arbitrarily small. The force on an atom  $\mathbf{k} \in \mathcal{L}$  is given by  $\mathbf{f}_{\mathbf{k}}(\mathbf{q}) = -\frac{\partial E^M(\mathbf{q})}{\partial \mathbf{x}_{\mathbf{k}}}$ , and using equation (54) we obtain

$$\mathbf{f}_{\mathbf{k}} = 2CV_e \nabla \phi_1(\mathbf{x}_{\mathbf{k}}) - C^2 V_e \nabla \phi_2(\mathbf{x}_{\mathbf{k}}). \tag{55}$$

We note that the expression for force on any atom given by equation (55) is *local*.

In arriving at equation (54) we computed the directional derivative by perturbing the positions of atoms. An equivalent approach, instead, is to consider a rearrangement of the domain  $\Omega$ , which corresponds to taking inner variations of the energy functional in equation (51). Let  $\psi_\epsilon : \Omega \rightarrow \Omega'$  be infinitesimal deformations corresponding to the generator  $\Gamma(\mathbf{y})$ , given by  $\Gamma = \frac{d\psi_\epsilon}{d\epsilon} \Big|_{\epsilon=0}$ , such that  $\psi_0 = id$ . We constrain the generator such that  $\Gamma$  is a constant in the compact support of each  $\delta(\mathbf{y} - \mathbf{x}_{\mathbf{i}})$  for  $\mathbf{i} \in \mathcal{L}$  in order to ensure that the shape and strength of the regularized dirac distributions centered around the atomic positions remain unchanged. Let  $\mathbf{y}$  denote a point in  $\Omega$  whose image in  $\Omega'$  is  $\mathbf{y}' = \psi_\epsilon(\mathbf{y})$ . We first consider the energy functional  $I_1$ , which for infinitesimal rearrangements of the

domain results in a family of energy functionals given by

$$I_1(\psi_\epsilon) = \frac{1}{8\pi\alpha} \left\{ \alpha^2 \int_{\Omega'} |\nabla_{\mathbf{y}'} \phi_{1\epsilon}(\mathbf{y}')|^2 d\mathbf{y}' + \frac{\alpha^4}{2} \int_{\Omega'} \phi_{1\epsilon}^2(\mathbf{y}') d\mathbf{y}' - 8\pi\alpha \int_{\Omega'} b(\psi_\epsilon^{-1}(\mathbf{y}'); \mathbf{q}) \phi_{1\epsilon}(\mathbf{y}') d\mathbf{y}' \right. \\ \left. - \int_{\Omega'} \nabla_{\mathbf{y}'} \phi_{1\epsilon}(\mathbf{y}') \cdot \nabla_{\mathbf{y}'} \rho_{1\epsilon}(\mathbf{y}') d\mathbf{y}' - \int_{\Omega'} \frac{1}{2} \rho_{1\epsilon}^2(\mathbf{y}') d\mathbf{y}' \right\}. \quad (56)$$

where  $\phi_{1\epsilon}$  and  $\rho_{1\epsilon}$  are minimizers and maximizers of  $I_1(\psi_\epsilon)$ . Transforming the integrals back onto  $\Omega$ , we obtain

$$I_1(\psi_\epsilon) = \frac{1}{8\pi\alpha} \left\{ \alpha^2 \int_{\Omega} \frac{\partial y_j}{\partial y'_i} \frac{\partial \phi_{1\epsilon}(\psi_\epsilon(\mathbf{y}))}{\partial y_j} \frac{\partial \phi_{1\epsilon}(\psi_\epsilon(\mathbf{y}))}{\partial y_k} \frac{\partial y_k}{\partial y'_i} \det\left(\frac{\partial y'_l}{\partial y_m}\right) d\mathbf{y} \right. \\ \left. + \frac{\alpha^4}{2} \int_{\Omega} \phi_{1\epsilon}^2(\psi_\epsilon(\mathbf{y})) \det\left(\frac{\partial y'_l}{\partial y_m}\right) d\mathbf{y} - 8\pi\alpha \int_{\Omega} b(\mathbf{y}; \mathbf{q}) \phi_{1\epsilon}(\psi_\epsilon(\mathbf{y})) \det\left(\frac{\partial y'_l}{\partial y_m}\right) d\mathbf{y} \right. \\ \left. - \int_{\Omega} \frac{\partial y_j}{\partial y'_i} \frac{\partial \phi_{1\epsilon}(\psi_\epsilon(\mathbf{y}))}{\partial y_j} \frac{\partial \rho_{1\epsilon}(\psi_\epsilon(\mathbf{y}))}{\partial y_k} \frac{\partial y_k}{\partial y'_i} \det\left(\frac{\partial y'_l}{\partial y_m}\right) d\mathbf{y} - \frac{1}{2} \int_{\Omega} \rho_{1\epsilon}^2(\psi_\epsilon(\mathbf{y})) \det\left(\frac{\partial y'_l}{\partial y_m}\right) d\mathbf{y} \right\}. \quad (57)$$

We note that in taking the variation of  $I_1(\psi_\epsilon)$ , the terms arising from variations of  $\phi_{1\epsilon}$  and  $\rho_{1\epsilon}$  vanish as  $\phi_1 (= \phi_{10})$  and  $\rho_1 (= \rho_{10})$  satisfy the Euler-Lagrange equations of  $I_1 (= I_1(\psi_0))$ . The non-trivial contributions to variation of  $I_1(\psi_\epsilon)$  come from variations of  $\det\left(\frac{\partial y'_l}{\partial y_m}\right)$  and  $\frac{\partial y_k}{\partial y'_i}$ . We first note the following identities which will be used subsequently:

$$\frac{d}{d\epsilon} \left\{ \frac{\partial y_i}{\partial y'_j} \right\} \Big|_{\epsilon=0} = - \frac{\partial y_i}{\partial y'_k} \left( \frac{d}{d\epsilon} \left\{ \frac{\partial \psi_{\epsilon k}}{\partial y_l} \right\} \right) \frac{\partial y_l}{\partial y'_j} \Big|_{\epsilon=0} \\ = - \frac{\partial \Gamma_i}{\partial y_j} \quad \left( \text{Note: } \frac{\partial y_i}{\partial y'_j} \Big|_{\epsilon=0} = \delta_{ij} \right), \quad (58)$$

$$\frac{d}{d\epsilon} \left\{ \det\left(\frac{\partial y'_l}{\partial y_m}\right) \right\} \Big|_{\epsilon=0} = \det\left(\frac{\partial y'_l}{\partial y_m}\right) \frac{\partial y_j}{\partial y'_i} \left( \frac{d}{d\epsilon} \left\{ \frac{\partial \psi_{\epsilon i}}{\partial y_j} \right\} \right) \Big|_{\epsilon=0} \\ = \frac{\partial \Gamma_j}{\partial y_j}. \quad (59)$$

Using the above identities, the Gâteaux derivative of the energy functional  $I_1$  is given by

$$\frac{dI_1(\psi_\epsilon)}{d\epsilon} \Big|_{\epsilon=0} = \int_{\Omega} W_1 \frac{\partial \Gamma_i}{\partial y_i} d\mathbf{y} - \frac{\alpha}{4\pi} \int_{\Omega} \frac{\partial \phi_1}{\partial y_i} \frac{\partial \phi_1}{\partial y_j} \frac{\partial \Gamma_i}{\partial y_j} d\mathbf{y} \\ + \frac{1}{8\pi\alpha} \int_{\Omega} \left( \frac{\partial \phi_1}{\partial y_i} \frac{\partial \rho_1}{\partial y_j} + \frac{\partial \rho_1}{\partial y_i} \frac{\partial \phi_1}{\partial y_j} \right) \frac{\partial \Gamma_i}{\partial y_j} d\mathbf{y}, \quad \text{where} \quad (60) \\ W_1 = \frac{1}{8\pi\alpha} \left\{ \alpha^2 |\nabla \phi_1|^2 + \frac{\alpha^4}{2} \phi_1^2 - \nabla \phi_1 \cdot \nabla \rho_1 - \frac{1}{2} \rho_1^2 \right\}.$$

In the above calculation, we have used  $\text{div}\Gamma = 0$  in the compact support of  $b$  (as  $\Gamma$  is a constant in support of each  $\delta(\mathbf{y} - \mathbf{x}_i)$  for  $i \in \mathcal{L}$ ) to drop the term  $\int_{\Omega} b\phi_1 \text{div}\Gamma d\mathbf{y}$ . On similar lines we compute the Gâteaux derivative of the energy functional  $I_2$  to be

$$\begin{aligned} \left. \frac{dI_2(\psi_{\epsilon})}{d\epsilon} \right|_{\epsilon=0} &= \int_{\Omega} W_2 \frac{\partial \Gamma_i}{\partial y_i} d\mathbf{y} - \frac{\alpha}{2\pi} \int_{\Omega} \frac{\partial \phi_2}{\partial y_i} \frac{\partial \phi_2}{\partial y_j} \frac{\partial \Gamma_i}{\partial y_j} d\mathbf{y} \\ &\quad + \frac{1}{16\pi\alpha} \int_{\Omega} \left( \frac{\partial \phi_2}{\partial y_i} \frac{\partial \rho_2}{\partial y_j} + \frac{\partial \rho_2}{\partial y_i} \frac{\partial \phi_2}{\partial y_j} \right) \frac{\partial \Gamma_i}{\partial y_j} d\mathbf{y}, \quad \text{where} \quad (61) \\ W_2 &= \frac{1}{16\pi\alpha} \left\{ 4\alpha^2 |\nabla \phi_2|^2 + 8\alpha^4 \phi_2^2 - \nabla \phi_2 \cdot \nabla \rho_2 - \frac{1}{2} \rho_2^2 \right\}. \end{aligned}$$

From equations (60) and (61), the generalized force corresponding to  $E^M$  is given by

$$\begin{aligned} \left. \frac{dE(\psi_{\epsilon})}{d\epsilon} \right|_{\epsilon=0} &= \int_{\Omega} E_{ij} \frac{\partial \Gamma_i}{\partial y_j} d\mathbf{y}, \quad \text{where} \\ E_{ij} &= (W_1 + W_2) \delta_{ij} - \frac{\alpha}{2\pi} \left( CV_e \frac{\partial \phi_1}{\partial y_i} \frac{\partial \phi_1}{\partial y_j} - C^2 V_e \frac{\partial \phi_2}{\partial y_i} \frac{\partial \phi_2}{\partial y_j} \right) \\ &\quad + \frac{1}{16\pi\alpha} \left\{ 4CV_e \left( \frac{\partial \phi_1}{\partial y_i} \frac{\partial \rho_1}{\partial y_j} + \frac{\partial \rho_1}{\partial y_i} \frac{\partial \phi_1}{\partial y_j} \right) - C^2 V_e \left( \frac{\partial \phi_2}{\partial y_i} \frac{\partial \rho_2}{\partial y_j} + \frac{\partial \rho_2}{\partial y_i} \frac{\partial \phi_2}{\partial y_j} \right) \right\}. \quad (62) \end{aligned}$$

The above expression for generalized forces corresponding to the outer minimization problem in equation (53), which is *local*, is the Eshelby representation of configurational forces. In this article we refer to this form as the Eshelby form of generalized forces. We note that equations (54) and (62) are equivalent when  $\psi_{\epsilon} : \Omega \rightarrow \Omega$ , which can be verified by integrating by parts the expression in equation (62), and using the Euler-Lagrange equations for potentials. However, when  $\psi_{\epsilon} : \Omega \rightarrow \Omega'$ , then the Eshelby form alone gives the correct generalized force which also accounts for the change in the domain. In the quasi-continuum reduction to follow in section 5 the elastic effects in coarse-grained regions of the triangulation arise from the change in the shape and size of unit cells representing the Cauchy-Born deformation. These elastic effects are naturally captured by the Eshelby form, and therein lies its need and usefulness.

#### 4.2 Lennard-Jones kernels

We now proceed to the local reformulation of kernels of the form  $\frac{1}{|\mathbf{x}_i - \mathbf{x}_j|^m}$  where  $m$  is a positive integer. Lennard-Jones interatomic potential (Lennard-Jones, 1924) is an example of a widely used potential that uses kernels of this form, alongside some EAM potentials (cf. e. g. Sutton & Chen (1990)). We seek to construct the partial differential equation whose Green's function is the kernel  $\frac{1}{|\mathbf{y} - \mathbf{y}'|^m}$ . We note that the Green's function of Laplace operator in three-dimensions is  $\frac{1}{|\mathbf{y} - \mathbf{y}'|}$ . But constructing a linear differential operator whose Green's function is  $\frac{1}{|\mathbf{y} - \mathbf{y}'|^m}$  for any generic  $m$  is beyond reach, at

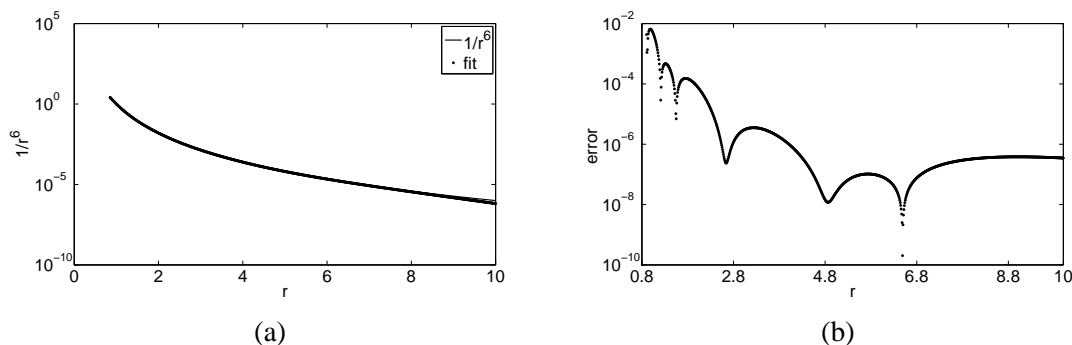


Fig. 5. (a) A fit for kernel  $\frac{1}{r^6}$  with an approximate kernel of the form  $ae^{-\alpha r} + b\frac{e^{-(\beta r)}}{r} + c\frac{e^{-(\gamma r)}}{r} + d\frac{e^{-(\lambda r)}}{r}$ ; (b) Absolute error in the approximation. Cusps in the error plot are points where the error changes sign.

least to the best of our knowledge. Thus we seek to find a good approximation for these kernels which can in turn be reformulated in a local form. We require this approximation to be accurate in the domain of influence of the potential—typically in the range  $0.85a < |\mathbf{y} - \mathbf{y}'| < Ca$ ,  $C \in \mathbb{Z}$ , where  $a$  is the nearest neighbor interatomic spacing of an undeformed lattice. The lower limit of this range guarantees that the energetics are accurate even up to 15% compressive strains and the value of the upper-limit  $C$  is chosen based on the decay of the potential. We consider an approximation of the form

$$\frac{1}{|\mathbf{y} - \mathbf{y}'|^m} \approx \sum_{j=1}^{M_0} A_j \frac{e^{-\alpha_j |\mathbf{y} - \mathbf{y}'|}}{4\pi |\mathbf{y} - \mathbf{y}'|} + \sum_{k=1}^{M_1} B_k e^{-\beta_k |\mathbf{y} - \mathbf{y}'|}, \quad (63)$$

where  $A_j, \alpha_j$  for  $j = 1 \dots M_0$  and  $B_k, \beta_k$  for  $k = 1 \dots M_1$  are constants that are fitted to best approximate the kernel. We note that potentials associated with kernels of the form  $\frac{e^{-\alpha |\mathbf{y} - \mathbf{y}'|}}{4\pi |\mathbf{y} - \mathbf{y}'|}$  are often referred to as Yukawa potentials (cf. e. g. [Ashcroft & Mermin \(1976\)](#)). To test the accuracy of this approximation we consider two test cases with  $m = 6$  and  $m = 12$  that correspond to the Lennard-Jones interatomic potential. Figures 5, 6 demonstrate the accuracy of this approximation, where by just using four terms in the power series we obtain a good approximation to the desired kernels. Table 1 provides the coefficients corresponding to these approximations, where the relative  $\ell^2$  error of these approximations, calculated using discrete points in  $[0.85a, 10a]$  with a uniform spacing of  $0.01a$ , is less than 0.01 in both cases.

Following the ideas developed in section 4.1, we replace the atoms by regularized dirac distributions and the interatomic interaction energy corresponding to a  $\frac{1}{|\mathbf{x}_i - \mathbf{x}_j|^m}$  kernel is then given by

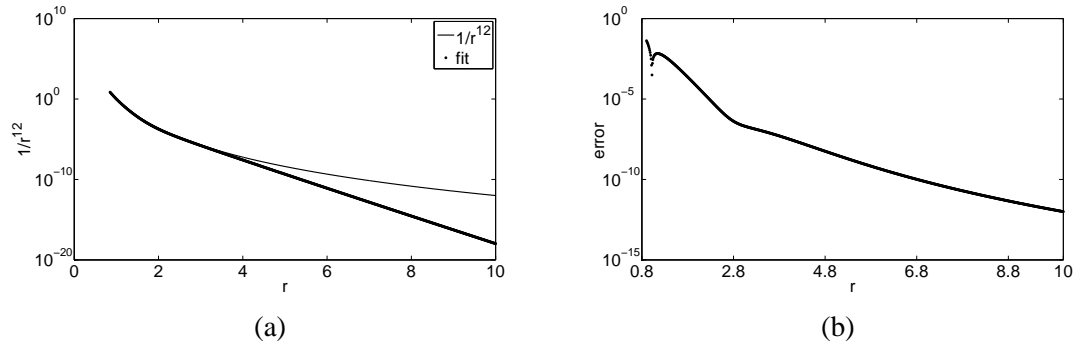


Fig. 6. (a) A fit for kernel  $\frac{1}{r^{12}}$  with an approximate kernel of the form  $ae^{-\alpha r} + b\frac{e^{-(\beta r)}}{r} + c\frac{e^{-(\gamma r)}}{r} + d\frac{e^{-(\lambda r)}}{r}$ ; (b) Absolute error in the approximation.

Table 1

Table of coefficients for an approximate fitting of  $\frac{1}{r^6}$  and  $\frac{1}{r^{12}}$  kernels with a kernel of the form  $ae^{-\alpha r} + b\frac{e^{-(\beta r)}}{r} + c\frac{e^{-(\gamma r)}}{r} + d\frac{e^{-(\lambda r)}}{r}$ .

coefficients of fit for kernel $\frac{1}{r^6}$				coefficients of fit for kernel $\frac{1}{r^{12}}$			
a	0.002484	$\alpha$	0.8252	a	$1.349 * 10^7$	$\alpha$	18.1135
b	14.11	$\beta$	3.4262	b	225.2	$\beta$	7.2092
c	547.5	$\gamma$	7.0597	c	$2.6 * 10^4$	$\gamma$	10.608
d	0.3833	$\lambda$	1.6154	d	0.4877	$\lambda$	3.8377

$$\begin{aligned}
 E(\mathbf{q}) &= \int_{\Omega} \int_{\Omega} b(\mathbf{y}; \mathbf{q}) \frac{1}{|\mathbf{y} - \mathbf{y}'|^m} b(\mathbf{y}'; \mathbf{q}) d\mathbf{y} d\mathbf{y}' \\
 &\approx \sum_{j=1}^{M_0} A_j \int_{\Omega} \int_{\Omega} b(\mathbf{y}; \mathbf{q}) \frac{e^{-\alpha_j |\mathbf{y} - \mathbf{y}'|}}{4\pi |\mathbf{y} - \mathbf{y}'|} b(\mathbf{y}'; \mathbf{q}) d\mathbf{y} d\mathbf{y}' + \sum_{k=1}^{M_1} B_k \int_{\Omega} \int_{\Omega} b(\mathbf{y}; \mathbf{q}) e^{-\beta_k |\mathbf{y} - \mathbf{y}'|} b(\mathbf{y}'; \mathbf{q}) d\mathbf{y} d\mathbf{y}'.
 \end{aligned} \tag{64}$$

To keep the expressions simple, we will represent the second series of exponential kernels in equation (64) by  $E^{exp}(\mathbf{q})$  whose local reformulation is already established in section 4.1. We denote by  $\phi_j(\mathbf{y}; \mathbf{q})$  the convolution  $\int \frac{e^{-\alpha_j |\mathbf{y} - \mathbf{y}'|}}{4\pi |\mathbf{y} - \mathbf{y}'|} b(\mathbf{y}'; \mathbf{q}) d\mathbf{y}'$ ,  $j = 1, \dots, M_0$ . Taking the Fourier transform of the above expression we obtain

$$(|\mathbf{k}|^2 + \alpha_j^2) \hat{\phi}_j(\mathbf{k}) = \hat{b}(\mathbf{k}) \quad j = 1, \dots, M_0. \tag{65}$$

Taking the inverse Fourier transform we obtain the Helmholtz equation

$$(-\nabla^2 + \alpha_j^2) \phi_j(\mathbf{y}; \mathbf{q}) = b(\mathbf{y}; \mathbf{q}) \quad j = 1, \dots, M_0. \tag{66}$$

The energy in equation (64) can now be reformulated into a local form using the variational form of equation (66), and is given by

$$E(\mathbf{q}) = \sum_{j=1}^{M_0} 2A_j I_j(\mathbf{q}) + E^{exp}(\mathbf{q}), \quad \text{where}$$

$$I_j(\mathbf{q}) = - \min_{\varphi_j \in H_0^1(\Omega)} \left\{ \frac{1}{2} \int_{\Omega} |\nabla \varphi_j|^2 d\mathbf{y} + \frac{\alpha_j^2}{2} \int_{\Omega} \varphi_j^2 d\mathbf{y} - \int_{\Omega} b(\mathbf{q}) \varphi_j d\mathbf{y} \right\} \quad j = 1, \dots, M_0. \quad (67)$$

Further  $\phi_j = \arg \min I_j$ . Following on similar lines as in section 4.1 the Eshelby form of the generalized force for infinitesimal deformations corresponding to the generator  $\Gamma$  is given by

$$\frac{dE(\psi_\epsilon)}{d\epsilon} \Big|_{\epsilon=0} = \sum_{j=1}^{M_0} 2A_j \frac{dI_j(\psi_\epsilon)}{d\epsilon} \Big|_{\epsilon=0} + \frac{dE^{exp}(\psi_\epsilon)}{d\epsilon} \Big|_{\epsilon=0}, \quad \text{where}$$

$$\frac{dI_j(\psi_\epsilon)}{d\epsilon} \Big|_{\epsilon=0} = - \int_{\Omega} \left\{ \frac{1}{2} |\nabla \phi_j|^2 + \frac{\alpha_j^2 \phi_j^2}{2} \right\} \frac{\partial \Gamma_i}{\partial y_i} d\mathbf{y} + \int_{\Omega} \frac{\partial \phi_j}{\partial y_i} \frac{\partial \phi_j}{\partial y_k} \frac{\partial \Gamma_i}{\partial y_k} d\mathbf{y} \quad j = 1, \dots, M_0. \quad (68)$$

Hence the energy as well as force expressions are now expressed in a local form which are amenable to quasi-continuum reduction, and is discussed in the next section.

## 5 Quasi-continuum reduction

The energetics of a material system, following the local reformulation of extended interactions discussed in section 4, is described by various fields, namely, the displacement field of atomic positions and potential fields that appear in the variational formulation (cf. equation (53)). The nature of the displacement field is such that it varies rapidly near the core of a defect but becomes smooth away from the core where the response is elastic. Potential fields on the other hand exhibit oscillations on the length-scale of the lattice parameter. This follows from oscillations in the forcing term,  $b(\mathbf{q})$ , on the lattice length-scale. In regions away from the defect-core, where the displacement field is smoothly varying, the fine-scale oscillations in potential fields exhibit a well characterized structure. In these regions potential fields are determined to leading order by a periodic calculation using the Cauchy-Born deformation. This follows from a formal result in [Blanc et al. \(2002\)](#), where this property has been shown for a class of non-linear functionals. We exploit this structure in potential fields to achieve the quasi-continuum reduction of the local field formulation proposed in section 4. The key ideas behind this quasi-continuum reduction have first been proposed in the context of orbital-free density functional theory in [Gavini et al. \(2007\)](#). Here, we revisit these ideas in the context of empirical interatomic potentials with the focus on demonstrating the method being a systematic numerical coarse-graining scheme devoid of the inconsistencies in previous QC formulations.

The quasi-continuum reduction of field formulation is realized by coarse-graining the

various fields that appear in the formulation using three unstructured finite-element triangulations with *linear* shape-functions:

- (i) a triangulation  $T_{h_1}$  of selected representative atoms in the usual manner of QC, which is labeled as *atomic mesh*;
- (ii) a triangulation  $T_{h_3}$ , subatomic close to lattice defects and increasingly coarser away from the defects, which is labeled as *potential-mesh*.
- (iii) an uniformly subatomic triangulation  $T_{h_2}$  to capture the fine-scale oscillations in potential fields, which is labeled as *fine-mesh*.

We further denote  $\mathcal{L}_{h_1}$  as the set containing the representative atoms, which correspond to the nodes of triangulation  $T_{h_1}$ . A schematic of the hierarchy of meshes in one dimension is shown in figure 7. For convenience, these triangulations are restricted in such a way that  $T_{h_3}$  is a sub-grid of  $T_{h_1}$  and  $T_{h_2}$  is a sub-grid of  $T_{h_3}$ . The corresponding finite-element approximation spaces are denoted by  $X^{h_1}$ ,  $X^{h_2}$  and  $X^{h_3}$ . To demonstrate the main ideas behind quasi-continuum reduction, we consider the energy of a system described by exponential kernels. We recall from section 4.1 that the local reformulation of such an energy is given by

$$E_0^M = \min_{\mathbf{q} \in X} \min_{\substack{\varphi_1 \in Y \\ \varphi_2 \in Y \\ \varrho_2 \in Y}} \max_{\substack{\varphi_2 \in Y \\ \varrho_1 \in Y}} \int_{\Omega} L(\varphi_1, \varrho_1, \varphi_2, \varrho_2; \mathbf{q}) d\mathbf{y}. \quad (69)$$

where  $L$  denotes the Lagrangian given in equation (51). In the above expression  $Y$  denotes a suitable function space which is  $H_0^1(\Omega)$  for non-periodic problems on domain  $\Omega$ , or  $H_{Per}^1(Q)$  for periodic problems on a supercell  $Q$ . We decompose the potentials as

$$\begin{aligned} \varphi_1 &= \varphi_{10} + \varphi_{1c}, & \varphi_2 &= \varphi_{20} + \varphi_{2c}, \\ \varrho_1 &= \varrho_{10} + \varrho_{1c}, & \varrho_2 &= \varrho_{20} + \varrho_{2c}, \end{aligned} \quad (70)$$

where  $(\varphi_{10}, \varphi_{20}, \varrho_{10}, \varrho_{20})$  denote the predictors for the potential fields and  $(\varphi_{1c}, \varphi_{2c}, \varrho_{1c}, \varrho_{2c})$  denote the corresponding correctors. The predictors for the potential fields are computed by performing a periodic calculation on a unit cell in every element of  $T_{h_1}$  and mapped on to  $T_{h_2}$ . The resulting fields are in general not continuous across the boundaries of elements of  $T_{h_1}$  and we use a  $L^2 \rightarrow H^1$  map to obtain conforming fields. One way to obtain such a map is to average the fields across the boundaries of elements of  $T_{h_1}$  (cf. e. g. [Gavini et al. \(2007\)](#)). In regions away from the defect-core, where the deformation field is slowly varying, the nature of the corrector fields is such that they do not exhibit fine-scale oscillations on the length-scale of the lattice parameter. This is justified in the sequel to this article ([Gavini & Liu \(2010\)](#)) using formal multi-scale analysis, where a more general case of non-linear functionals is treated. Thus, corrector fields can now be accurately represented on a coarse-grained triangulation, like  $T_{h_3}$ , which has subatomic resolution in regions of rapid variation of the deformation field and is coarse-grained elsewhere.

The unknowns in the formulation comprising of the coarse-grained displacement field and

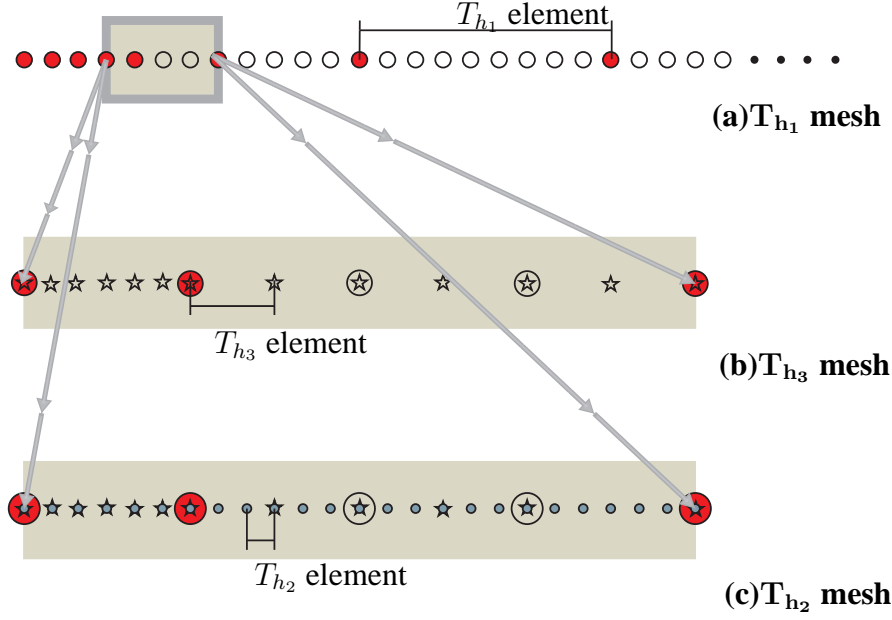


Fig. 7. Schematic sketch of meshes: (a) Shows the atomic-mesh, which has atomistic resolution in regions of interest and is coarse-grained elsewhere. The circles in red denote representative atoms. (b) Shows the potential-mesh, used to represent the corrections to the predictor of potential fields. The stars in black represent the nodes of this mesh. It is subatomic in regions of interest and coarse-grains to become superatomic. (c) Shows the fine-mesh which resolves the predictor for the potential fields. The nodes of this mesh are small circles in blue. Unlike  $T_{h_1}$  and  $T_{h_3}$  which are coarse-grained,  $T_{h_2}$  is a uniform subatomic mesh everywhere.

correctors for potential fields are computed from the constrained saddle-point problem:

$$E_0^{hM} = \min_{\mathbf{q}^h \in X_{h_1}} \min_{\substack{\varphi_{1c}^h \in X_{h_3} \\ \varphi_{2c}^h \in X_{h_3}}} \max_{\substack{\varphi_{2c}^h \in X_{h_3} \\ \varrho_{1c}^h \in X_{h_3}}} \int_{\Omega} L(\varphi_{10}^h + \varphi_{1c}^h, \varrho_{10}^h + \varrho_{1c}^h, \varphi_{20}^h + \varphi_{2c}^h, \varrho_{20}^h + \varrho_{2c}^h; \mathbf{q}^h) dy. \quad (71)$$

Since the predictors for the potential fields are represented on a uniformly subatomic mesh  $T_{h_2}$ , the computation of the energy still has a complexity commensurate with the size of  $T_{h_2}$ . In regions of slowly varying deformations, which corresponds to coarse-grained regions of  $T_{h_1}$  and  $T_{h_3}$ , the predictor fields are accurate representations of potential fields and the corrector fields are very small compared to the predictors. We exploit this fact to introduce quadrature rules on integrals that reduce all the computations to the complexity of the coarse-grained mesh  $T_{h_3}$ . The precise form of the integration rule for an element  $e$  in the triangulation  $T_{h_3}$  is

$$\int_e f(\mathbf{y}) dy \approx |e| \langle f \rangle_{D_e}, \quad (72)$$

where  $|e|$  is the volume of element  $e$ ,  $D_e$  is the unit cell of an atom if such cell is contained in  $e$  or  $e$  otherwise, and  $\langle f \rangle_{D_e}$  is the average of  $f$  over  $D_e$ . Using (72), integration over

the entire domain can be written as,

$$\int_{\Omega} f(\mathbf{y})d\mathbf{y} = \sum_{e \in T_{h_3}} \int_e f(\mathbf{y})d\mathbf{y} \approx \sum_{e \in T_{h_3}} |e| \langle f \rangle_{D_e}, \quad (73)$$

reducing all computations to have a complexity commensurate with the size of  $T_{h_3}$ . We note that this quadrature rule is exact for elements of  $T_{h_3}$  which are smaller than the unit cell, which we are labeled *subatomic* elements. The approximation is only introduced in elements that are larger than a unit cell, labeled as *superatomic* elements. The nature of coarse-graining in triangulations is such that these superatomic elements lie in regions of smooth deformations where the corrector fields are very small compared to the predictor fields. Thus, the integrand of equation (72) is a rapidly oscillating function with a small correction on the scale of the element. Hence, equation (72), for regions away from the core of a defect, denotes a zero order quadrature rule for rapidly oscillating functions.

Following the introduction of quadrature rules, predictor fields no longer need to be represented on a uniformly subatomic mesh everywhere in the domain, which is memory intensive. In the superatomic elements of  $T_{h_3}$ , where the quadrature approximation is used, it suffices to represent predictor fields on an auxiliary unit cell. This is demonstrated in figure 8, where  $T_{h_2}$  now represents a triangulation of disjoint simply connected domains formed from unit cells in each element of  $T_{h_3}$ . In the subatomic elements of  $T_{h_3}$ ,  $T_{h_2}$  represents a uniform triangulation of the underlying domain. In the superatomic elements of  $T_{h_3}$ ,  $T_{h_2}$  represents a uniform triangulation of the unit cell contained in the  $T_{h_3}$  element. Further, the triangulations are constructed such that for affine deformations of a perfect lattice the following are satisfied:

M1: Each simply connected domain representing the predictor fields has an energy density equal to that of a unit cell. This restriction ensures that the energy of the system is computed exactly for a perfect lattice undergoing affine deformations.

M2: The integration rule is exact for all superatomic elements of  $T_{h_3}$  lying in the compact support of any shape-function of  $T_{h_1}$  that also contains one or more subatomic elements of  $T_{h_3}$ .

We remark that it is always possible to choose triangulations that satisfy these restrictions in one- two- and three-dimensions. M1 can be satisfied by a careful choice of the boundaries between subatomic and superatomic elements. In one-dimension, it is sufficient to choose this boundary at the atomic position or at the mid-point between two atoms. In higher dimensions, it is sufficient to choose these boundaries to be planes of symmetry of the lattice. To satisfy M2, it is sufficient to choose the superatomic elements of  $T_{h_3}$ , lying in the compact support of any shape-function of  $T_{h_1}$  that also contains one or more subatomic elements of  $T_{h_3}$ , to have element boundaries that are planes of symmetry of the lattice. In one-dimension, it suffices to choose a triangulation such that these superatomic elements have half-integer number of atoms as shown in figure 9.

We now turn our attention to investigate if the quasi-continuum reduction of field for-

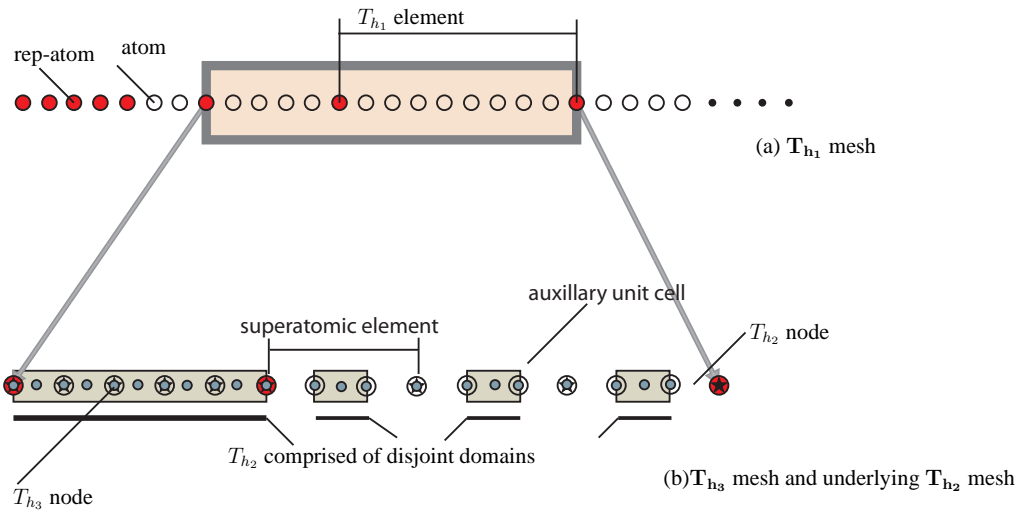


Fig. 8. Schematic showing reduction in computational complexity upon introduction of quadrature rules. (a) Atomic-mesh: circles denote atomic sites; circles in red denote representative atoms (rep-atoms). (b) Potential-mesh and fine-mesh: small circles in blue denote  $T_{h_2}$  nodes; stars denote  $T_{h_3}$  nodes. The disjoint clusters representing the  $T_{h_2}$  mesh is enclosed in a light green box.

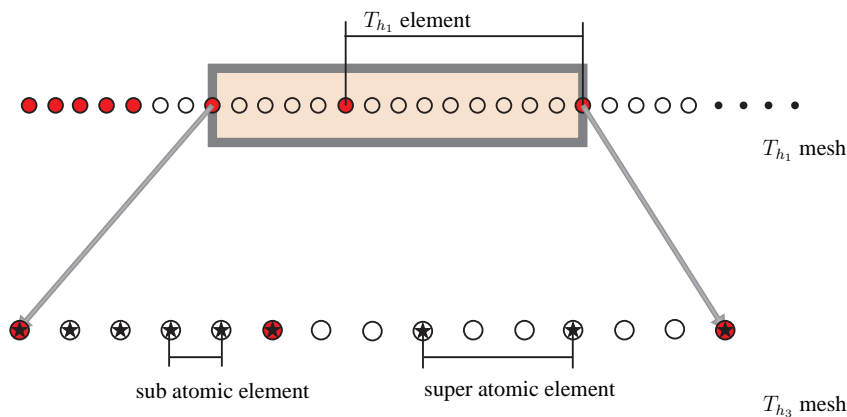


Fig. 9. A triangulation showing a superatomic element and a subatomic element in the  $T_{h_3}$  mesh. The quadrature rule is exact in such a region.

mulations proposed here satisfies the consistency conditions laid out in section 2 (C1 and C2) which are necessary for systematic convergence of numerical approximations. To this end, we consider a perfect crystal undergoing an affine deformation given by  $\mathbf{F}$ , and denote our domain of analysis by a super cell  $Q$  containing  $N_0$  atoms. Further, we denote a unit cell in the lattice by  $U$ . The suitable function space for the corrector fields is  $H_{per}^1(Q)$ , which represents periodic boundary conditions on corrector fields. Further, we investigate the problem in the limit  $h_2 \rightarrow 0$ , where approximation errors in predictor fields are not considered, as we are interested in approximation errors corresponding to the coarse-grained fields. We note that the saddle-point problem given by equation (71) returns a trivial solution for the corrector fields. The energy is thus given by

$$\begin{aligned}
 E_0^{hM} &= \min_{\substack{\varphi_{1c}^h \in X_{h_3} \\ \varrho_{2c}^h \in X_{h_3}}} \max_{\substack{\varphi_{2c}^h \in X_{h_3} \\ \varrho_{1c}^h \in X_{h_3}}} \int_Q L(\varphi_{10} + \varphi_{1c}^h, \varrho_{10} + \varrho_{1c}^h, \varphi_{20} + \varphi_{2c}^h, \varrho_{20} + \varrho_{2c}^h; \mathbf{F}) d\mathbf{y} \\
 &= \int_Q L(\varphi_{10}, \varrho_{10}, \varphi_{20}, \varrho_{20}; \mathbf{F}) d\mathbf{y} = \sum_{e \in T_{h_3}} |e| \langle L \rangle_{D_e} \\
 &= N_0 \int_U L(\varphi_{10}, \varrho_{10}, \varphi_{20}, \varrho_{20}; \mathbf{F}) d\mathbf{y}, \tag{74}
 \end{aligned}$$

where the last equality follows from the restriction M1 that each simply connected domain has an energy density equal to that of a unit cell. Equation (74) demonstrates that the quadrature rule used satisfies the consistency condition C1.

We now investigate whether the proposed quasi-continuum reduction of field formulations passes the patch test. The force on any representative node is given by replacing the generator in equation (62) by the shape-function associated with the representative node:

$$(\mathbf{f}_{\mathbf{K}}^{h_1})_i = - \int_Q E_{ij} \frac{\partial \Phi_{\mathbf{K}}^{h_1}}{\partial y_j} d\mathbf{y} \quad i = 1, 2, 3, \quad \mathbf{K} \in \mathcal{L}_{h_1}, \tag{75}$$

where  $(\mathbf{f}_{\mathbf{K}}^{h_1})_i$  denotes the force in the  $i^{\text{th}}$  direction on a representative node  $\mathbf{K}$  in the triangulation  $T_{h_1}$ ;  $\Phi_{\mathbf{K}}^{h_1}$  denotes the shape-function associated with the representative node  $\mathbf{K}$ . We remark that the shape-functions should be adjusted such that they are a constant in the support of each  $\delta(\mathbf{y} - \mathbf{x}_i)$  for  $i \in \mathcal{L}$  to preserve the shape and strength of the regularized dirac distribution. However, in a practical implementation of the method, the dirac distributions are often represented as point loads on the nodes of the triangulation, and the discreteness of the mesh provides the regularization. In such a case, as the measure of  $b$  is zero, the required condition on the shape-functions is trivially satisfied. We consider the following three cases to analyze the force expression: (i) the compact support of  $\Phi_{\mathbf{K}}^{h_1}$  contains only subatomic elements of  $T_{h_3}$ ; (ii) the compact support of  $\Phi_{\mathbf{K}}^{h_1}$  contains only superatomic elements of  $T_{h_3}$ ; (iii) the compact support of  $\Phi_{\mathbf{K}}^{h_1}$  contains both subatomic and superatomic elements of  $T_{h_3}$ .

*Case (i):* The force is given by

$$\begin{aligned}
 (\mathbf{f}_{\mathbf{K}}^{h_1})_i &= - \int_Q E_{ij} \frac{\partial \Phi_{\mathbf{K}}^{h_1}}{\partial y_j} d\mathbf{y} = \sum_{e \in T_{h_3}} \int_e E_{ij,j} \Phi_{\mathbf{K}}^{h_1} d\mathbf{y} \\
 &= \sum_{\mathbf{j} \in \mathcal{L}} (2CV_e \nabla \phi_1(\mathbf{x}_{\mathbf{j}}) - C^2 V_e \nabla \phi_2(\mathbf{x}_{\mathbf{j}}))_i \Phi_{\mathbf{K}}^{h_1}(\mathbf{x}_{\mathbf{j}}) = 0. \tag{76}
 \end{aligned}$$

The last equality follows from  $\nabla \phi_1(\mathbf{x}_{\mathbf{j}}) = 0$ ,  $\nabla \phi_2(\mathbf{x}_{\mathbf{j}}) = 0$ ,  $\mathbf{j} \in \mathcal{L}$ , for a lattice with affine deformation.

*Case (ii):* The force is given by

$$- (\mathbf{f}_{\mathbf{K}}^{h_1})_i = \sum_{e \in T_{h_3}} \int_e \mathbf{E}_{ij} \frac{\partial \Phi_{\mathbf{K}}^{h_1}}{\partial y_j} = \sum_{e \in T_{h_3}} |e| \langle \mathbf{E}_{ij} \frac{\partial \Phi_{\mathbf{K}}^{h_1}}{\partial y_j} \rangle_U \quad (77)$$

$$= \sum_{e \in T_{h_3}} |e| \langle \mathbf{E}_{ij} \rangle_U \langle \frac{\partial \Phi_{\mathbf{K}}^{h_1}}{\partial y_j} \rangle_U \quad (78)$$

$$= \langle \mathbf{E}_{ij} \rangle_U \sum_{e \in T_{h_3}} |e| \langle \frac{\partial \Phi_{\mathbf{K}}^{h_1}}{\partial y_j} \rangle_U = \langle \mathbf{E}_{ij} \rangle_U \int_Q \frac{\partial \Phi_{\mathbf{K}}^{h_1}}{\partial y_j} = 0. \quad (79)$$

We note that  $\langle \mathbf{E}_{ij} \frac{\partial \Phi_{\mathbf{K}}^{h_1}}{\partial y_j} \rangle_U = \langle \mathbf{E}_{ij} \rangle_U \langle \frac{\partial \Phi_{\mathbf{K}}^{h_1}}{\partial y_j} \rangle_U$  as  $\frac{\partial \Phi_{\mathbf{K}}^{h_1}}{\partial y_j}$  is a constant in every element  $e$  since  $\Phi_{\mathbf{K}}^{h_1}$  is a linear shape-function, and  $\int_Q \frac{\partial \Phi_{\mathbf{K}}^{h_1}}{\partial y_j} = 0$  as  $\Phi_{\mathbf{K}}^{h_1}$  has a compact support in  $Q$ .

*Case (iii):* Noting that the quadrature rule is exact for superatomic elements in this case from restriction M2, the integrals over unit cells can be replaced by integrals over the superatomic elements. This case then reduces to Case (i) from which it follows that  $(\mathbf{f}_{\mathbf{K}}^{h_1})_i = 0$ .

Thus, the quasi-continuum reduction of field formulations proposed here satisfies the consistency conditions necessary for systematic convergence of approximations.

## 6 Numerical Examples

We consider *nanoindentation* on a semi-infinite chain of atoms in a 1D setting as a test case to present the numerical accuracy and salient features of the proposed field formulation, and compare with the node-based formulations proposed in [Knap & Ortiz \(2001\)](#) and [Eidel & Stukowski \(2009\)](#). Though the nanoindentation problem in 1D does not reveal the critical phenomenon of dislocation nucleation which is observed in higher dimensions, we choose the problem in 1D as this allows us to consider a large enough system for which a full atomistic solution can be obtained in order to conduct a systematic study of approximation errors. To this end, we consider a chain consisting of 4110 atoms where one end of the chain is a free end, and the other end is fixed. The chain is extended beyond the fixed end to include atoms with fixed atomic positions that provide the environment of a semi-infinite chain. We use the Morse potential given by  $\bar{K}(|x_i - x_j|) = (1 - e^{-\alpha(|x_i - x_j| - x_e)})^2 - 1$  to describe the interatomic interactions. We choose the constants in the interatomic potential to be  $\alpha = 0.5$  and  $x_e = 2.8965$ , where units of all constants are in atomic units. We choose a cut-off radius of 50 atomic units for this potential, which ensures that relative errors from truncating the interatomic interactions are lower than the coarse-graining and quadrature errors that are investigated subsequently. The ground-state interatomic spacing of an infinite chain corresponding to these constants is  $a_0 = 1$ . We remark that our choice of constants is only a convenient choice for

numerical implementation and does not represent any particular physical system. In order to simulate the nanoindentation of the semi-infinite chain, we load the free end using an indenter which applies an external force on the atoms. Following [Knap & Ortiz \(2001\)](#), we consider the external force from the indenter to be given by  $AH(R-r)(R-r)^3$ , where ‘ $R$ ’ is the radius of the indenter, ‘ $r$ ’ is the distance between the center of the indenter and the atomic site and  $H(r)$  is the heavy-side function. In our simulations we choose  $R = 5$  and  $A = 0.5$ .

### 6.1 Node-based formulations

In order to compute the approximation errors, we first compute the ground-state energy and displacement field in the chain of atoms undergoing nanoindentation without introducing any approximations. The displacement field of an all-atom calculation is shown in figure 10, where  $X$  denotes the reference configuration and  $x$  denotes the deformed configuration. We note that the deformation in the chain is rapidly varying close to the indenter and at the fixed end, but is uniform in most parts of the chain which is characteristic of an elastic response. We now proceed to introduce the approximations in the quasi-continuum method and compute the corresponding errors. We first consider the node-based formulation in [Knap & Ortiz \(2001\)](#), and subsequently consider the formulation in [Eidel & Stukowski \(2009\)](#).

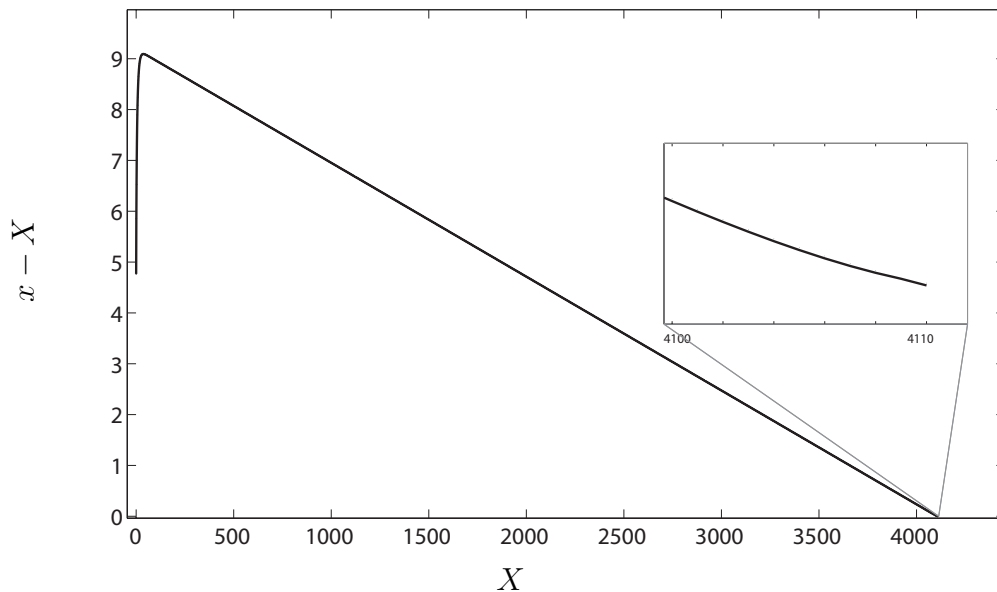


Fig. 10. Displacement field obtained from an all-atom simulation of a chain of atoms loaded by an indenter.

In the formulation proposed in [Knap & Ortiz \(2001\)](#), node-based cluster rules are introduced independently on forces and energy. We consider a sequence of triangulations of representative atoms (rep-atoms) to study the approximation properties of this formulation. We denote the set of triangulations by  $\mathcal{z}^h$ , indexed by the number of rep-atoms,

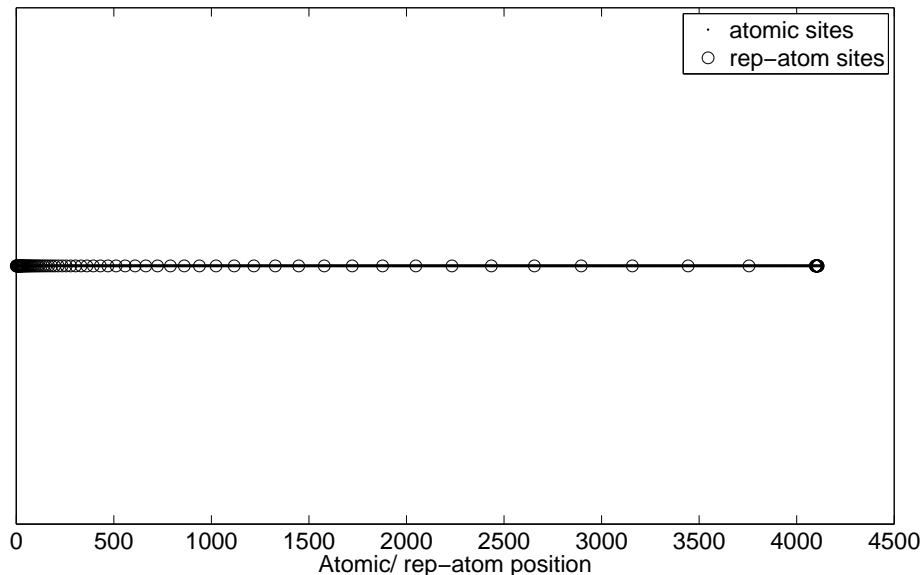
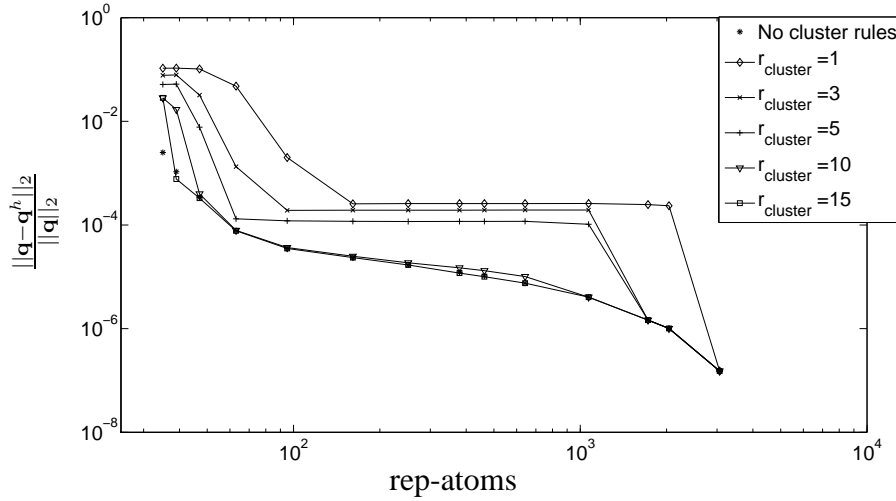


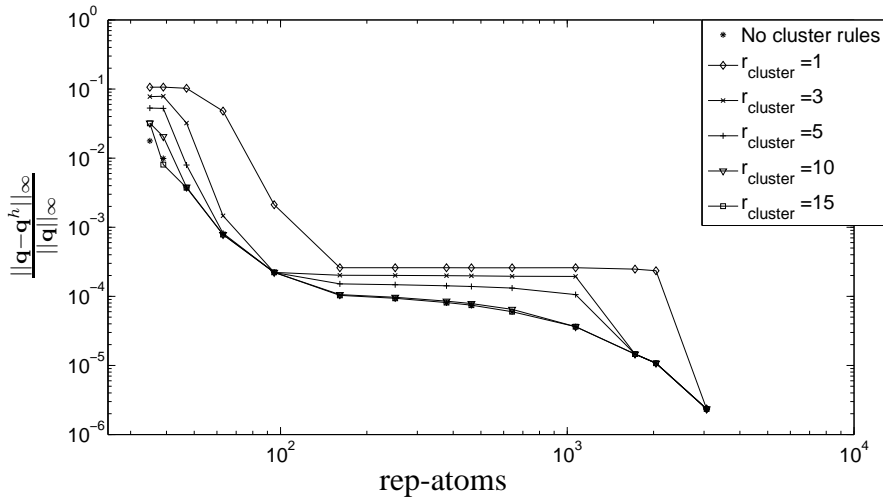
Fig. 11. Coarse grained mesh with 95 rep-atoms in a chain consisting of 4110 nominal number of atoms.

and are given by  $\mathcal{N}^h = \{35, 39, 47, 63, 95, 159, 251, 379, 463, 642, 1069, 3029, 3063\}$ . The sequence of triangulations are chosen such that finer triangulations form sub-grids of coarse triangulations, denoting a systematic refinement of the space of solutions. Figure 11 shows a triangulation with 95 rep-atoms. The triangulations are deliberately chosen to have rapid coarse-graining at the fixed end to study the robustness of various formulations of the quasi-continuum method. The convergence of quasi-continuum formulations are measured using relative errors in computed positions of atoms (displacement field) given by  $\frac{\|\mathbf{q}-\mathbf{q}^h\|_2}{\|\mathbf{q}\|_2}$ ,  $\frac{\|\mathbf{q}-\mathbf{q}^h\|_\infty}{\|\mathbf{q}\|_\infty}$ , and relative error in the energy given by  $\frac{|E-E^h|}{|E|}$ . Figure 12 shows the approximation errors for different number of rep-atoms and cluster radii. We note that these approximation errors can be decomposed into an error corresponding to coarse-graining (denoted by *coarse-graining error*), and another part corresponding to the approximations introduced through cluster summation rules (denoted by *quadrature error*). In the results shown in figure 12, the simulations performed without introducing cluster summation rules represent the coarse-graining error. Figure 13 demonstrates this decomposition and highlights the characteristics of the approximation errors. In our discussion, we will focus on the quadrature error as it is this error which determines the effectiveness of various formulations in the quasi-continuum method.

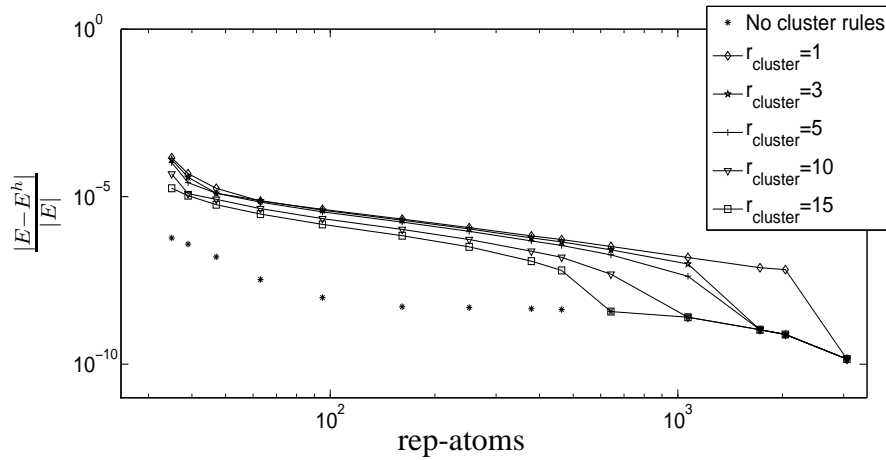
The nature of the approximation errors is such that three characteristic regions can be identified (cf. figure 13), at least for small cluster radii. In region I, corresponding to small number of rep-atoms, the approximation errors show a rapid drop with increasing number of rep-atoms. However, these errors plateau very quickly, and in region II no significant reduction of the error is observed upon further increase in the number of representative atoms. This region corresponds to a constant quadrature error. When the number of representative atoms become large enough that the clusters start overlapping,



(a) Relative root mean squared error in displacement field.



(b) Relative supremum error in displacement field.



(c) Relative error in total energy evaluation.

Fig. 12. Relative approximation errors in displacement field and total energy for formulation proposed in Knap & Ortiz (2001).

the quadrature errors vanish, which is expected—this denoted by region III. The stagnation of approximation errors in region II suggest that the node-based cluster summation rules are not providing a systematic convergence of the approximation error. These numerical results support our conclusions from the error estimates in section 3.1 that node-based cluster rules can result in large approximation errors for triangulations with rapid coarse-graining. We further note that, although the quadrature errors in displacement field systematically reduce with increasing cluster radii, the quadrature errors in the energy do not improve significantly. To explain this, we recall the error estimate for energy in equation (29) in section 3.1. The first term in this error estimate is independent of the cluster radius and will not reduce with increasing cluster radius.

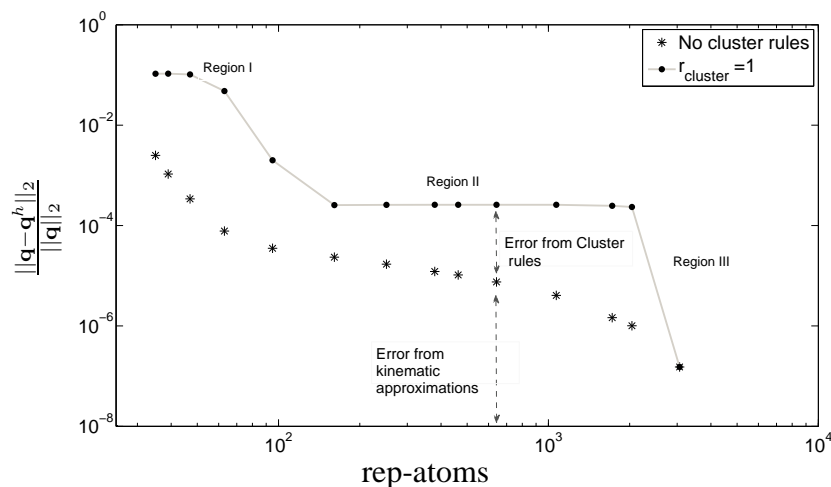


Fig. 13. Relative approximation error created due to kinematic constraints (coarse-graining errors) and cluster rules (quadrature errors).

We now proceed to study the approximation errors in the node-based formulation suggested in Eidel & Stukowski (2009), where node-based cluster summation rules are introduced on energy and the forces are computed as tangents of this approximate energy. As discussed in sections 2-3, this formulation fails the patch test and results in residual forces even for a perfect periodic system. These residual forces can become arbitrarily large with increasing coarse-graining and size of elements, and can seriously undermine the accuracy of the ground-state solution. It is suggested in Eidel & Stukowski (2009) that the effect of residual forces can be nullified by computing these residual forces for an initial configuration and subtracting them out as a dead load.

In our simulations we find, for rapid coarse-graining rates, the force iterations do not converge even after subtracting the dead loads as these dead loads are orders of magnitude larger than the physical forces. Most of the triangulations that have been used to study the approximation errors in the formulation proposed in Knap & Ortiz (2001) have rapid coarse-graining at the fixed end, and the force iterations for the formulation suggested in Eidel & Stukowski (2009) do not converge for these triangulations. Thus, we chose a different set of triangulations given by  $\mathcal{N}^h = \{74, 81, 95, 123, 179, 271, 399, 483, 662, 1089, 1743, 2059, 3083\}$ , where gradual coarse-graining is introduced on the fixed end. Figure 14 shows the approximation errors in displacement field and en-

ergy for the node-based formulation in Eidel & Stukowski (2009). As seen from the results, these errors are much larger than those corresponding to node-based formulation in Knap & Ortiz (2001), and unlike the previous case these errors do not reduce with increasing cluster radii. We note that these numerical results are in qualitative agreement with the error estimates in section 3 that suggest larger approximation errors in force computations using the formulation proposed in Eidel & Stukowski (2009) in comparison to the formulation proposed in Knap & Ortiz (2001)—the approximation errors in forces are  $O(a_1 - a_2)$  (equation 21) in node-based formulation in Knap & Ortiz (2001), whereas they are  $O(1)$  (equation 34) in node-based formulation in Eidel & Stukowski (2009). These larger errors in forces appear to result in larger approximation errors in the displacement field.

We further note that the spurious residual forces that arise in the formulation proposed in Eidel & Stukowski (2009) change with deformation in the chain. Therefore, for a complete nullification of these residual forces, the dead loads have to be computed in a self-consistent manner and updated. We now investigate if the self-consistent iteration converges. We conduct two sets of numerical tests: (i) with the cluster radius fixed at 10 and consider different number of rep-atoms given by  $\{74, 271, 662\}$ ; (ii) with the number of rep-atoms fixed at 483 and consider different cluster radii  $r = \{5, 10, 15\}$ . Figure 15 shows the results of this study, where the  $\ell^2$  norm of the difference in the dead loads in iterations  $i$  and  $i - 1$  of the self-consistent loop is presented. The self-consistent iteration does not necessarily converge, especially for small number of rep-atoms or small cluster radii. Numerical tests suggest that introducing linear mixing for the self-consistent iteration does not cure this deficiency.

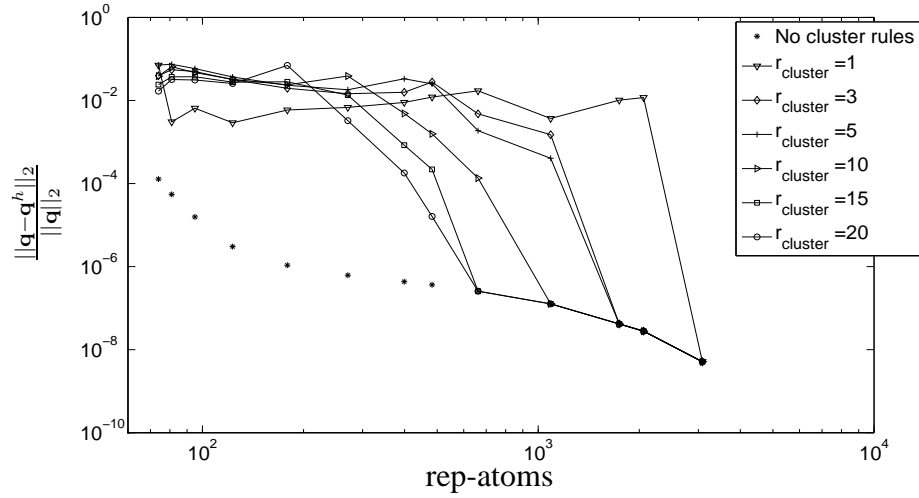
To summarize, the numerical results suggest that the approximation errors do not systematically converge in the node-based QC formulations. The quadrature errors are found to be orders of magnitude larger than the coarse-graining errors even for moderately large number of rep-atoms. Moreover, in the node-based QC formulation suggested in Eidel & Stukowski (2009), the self-consistent iteration which removes the effect of the residual forces may not always converge. We now proceed to study the approximation errors in the quasi-continuum reduction of the field formulation proposed in this article.

## 6.2 Field Formulation

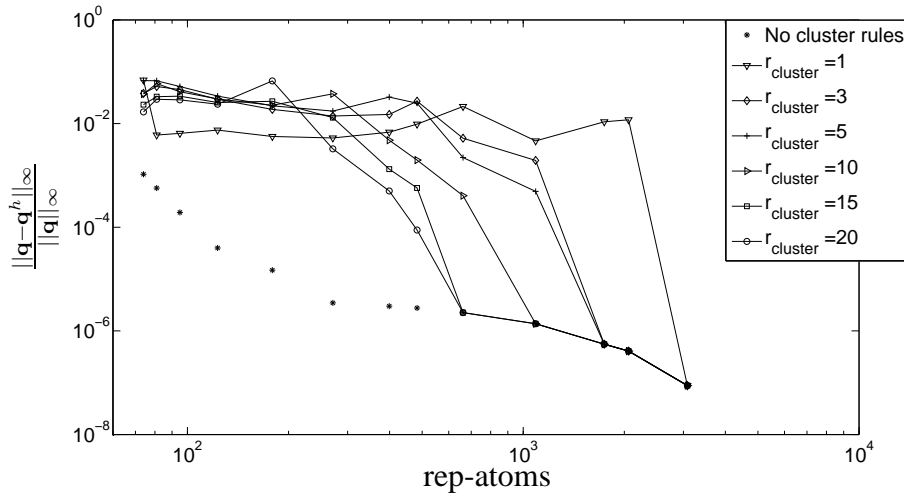
We numerically implemented the variational formulation in equation (53) for the nanoindentation problem in 1D. Using the same notation as in section 4.1, the potential created by a given configuration of atoms, represented by  $b(y; \mathbf{q})$ , is of the form

$$\phi(y; \mathbf{q}) = \int K(|y - y'|)b(y'; \mathbf{q})dy', \quad (80)$$

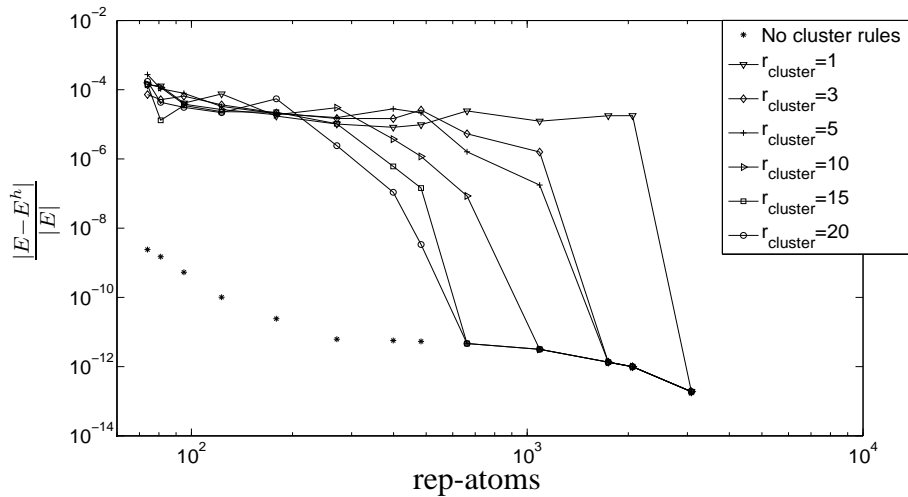
$$K(|y - y'|) = \left(1 - e^{-\alpha(|y-y'|-x_e)}\right)^2 - 1. \quad (81)$$



(a) Relative root mean squared error in displacement field.

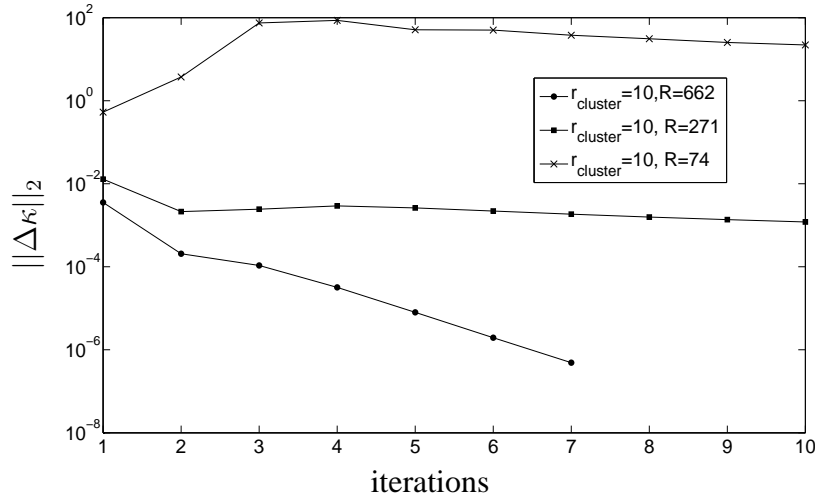


(b) Relative supremum error in displacement field.

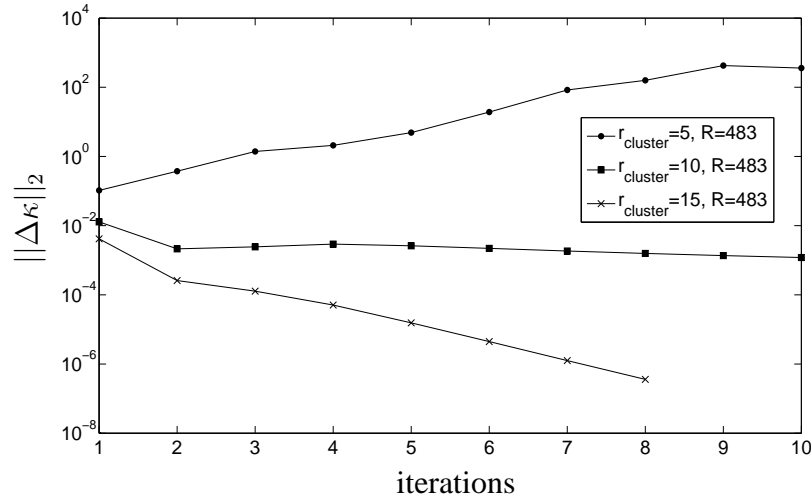


(c) Relative error in total energy evaluation.

Fig. 14. Relative approximation errors in displacement field and total energy for formulation proposed in Eidel & Stukowski (2009).



(a) Self consistent iteration results for a fixed cluster radius and different number of rep-atoms.



(b) Self consistent iteration results for a fixed number of rep-atoms and different cluster radii.

Fig. 15. Convergence study of the self-consistent iteration for residual force correction. Here  $\kappa(i)$  is the dead-load at the  $i^{\text{th}}$  iteration of the self consistent loop and  $\|\Delta\kappa(i)\|_2 = \|\kappa(i) - \kappa(i-1)\|_2$  is the  $\ell^2$  norm of change in dead-load against self-consistent iteration number.

Let  $\phi_1(y; \mathbf{q}) = \int e^{-\alpha|y-y'|} b(y'; \mathbf{q}) dy'$ , and  $\phi_2(y; \mathbf{q}) = \int e^{-2\alpha|y-y'|} b(y'; \mathbf{q}) dy'$ . The desired potential can now be represented as  $\phi(y) = -2e^{\alpha x_e} \phi_1(y) + e^{2\alpha x_e} \phi_2(y)$ . Evaluation of the potentials  $\phi_1, \phi_2$  requires an evaluation of convolution integrals with non-local kernels. Following the ideas presented in section 4, and noting that the Fourier Transform of  $e^{-\alpha|y|}$  in one dimension is  $\frac{2\alpha}{k^2 + \alpha^2}$ , these potentials can be reformulated into a local form using the following differential equations:

$$-\frac{d^2\phi_1(y; \mathbf{q})}{dy^2} + \alpha^2\phi_1(y; \mathbf{q}) = 2\alpha b(y; \mathbf{q}), \quad (82)$$

$$-\frac{d^2\phi_2(y; \mathbf{q})}{dy^2} + 4\alpha^2\phi_2(y; \mathbf{q}) = 4\alpha b(y; \mathbf{q}). \quad (83)$$

The problem of computing the ground-state solution can now be represented as the following saddle-point problem:

$$E_0 = \min_{\mathbf{q} \in \mathbb{R}^M} \min_{\varphi_1 \in \mathcal{X}} \max_{\varphi_2 \in \mathcal{X}} L(\varphi_1, \varphi_2, \mathbf{q}), \quad (84)$$

where  $\mathcal{X}$  denotes the appropriate function space corresponding to the boundary conditions,  $M$  denotes the number of rep-atoms, and

$$L(\varphi_1, \varphi_2; \mathbf{q}) = \frac{2e^{\alpha x_e}}{\alpha} \left( \frac{1}{2} \int |\nabla \varphi_1|^2 dy + \frac{\alpha^2}{2} \int \varphi_1^2 dy - 2\alpha \int \varphi_1(y) b(y; \mathbf{q}) dy \right) - \frac{e^{2\alpha x_e}}{2\alpha} \left( \frac{1}{2} \int |\nabla \varphi_2|^2 dy + 2\alpha^2 \int \varphi_2^2(y) dy - 4\alpha \int \varphi_2(y) b(y; \mathbf{q}) dy \right). \quad (85)$$

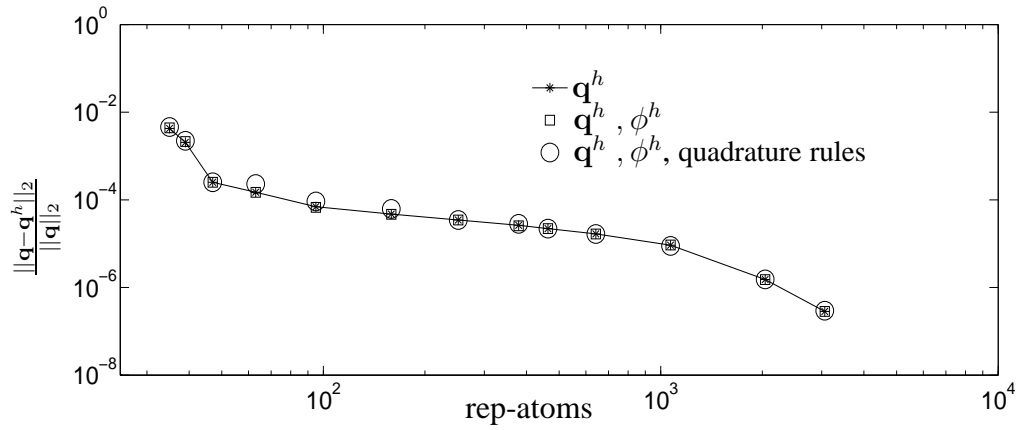
We have numerically implemented the quasi-continuum reduction of the above saddle-point problem following the ideas developed in section 5. As in section 5, we denote the triangulation of the representative atoms as  $T_{h_1}$  (atomic-mesh), the triangulation resolving the corrector fields as  $T_{h_3}$  (potential-mesh), and the triangulation resolving the predictor fields as  $T_{h_2}$  (fine-mesh). We chose the triangulations such that discretization errors in the computation of forces, which requires a numerical evaluation of gradients of potential fields, are below  $10^{-10}$ . We used a nested iterative scheme for solving the saddle-point problem in equation (84), where for every displacement field given by  $\mathbf{q}^h$  the potential fields are computed by solving the min – max problem on  $(\phi_1^h, \phi_2^h)$ . We used a sparse-representation iterative solver for solution of  $(\phi_1^h, \phi_2^h)$ , which is a linear problem, and a Levenberg-Marquardt iterative algorithm (cf. e. g. [Moré \(1977\)](#)) for solution of the non-linear problem corresponding to the minimization with respect to positions of atoms.

In order to determine the approximation errors in the proposed field formulation we have conducted three different studies. The first study considers coarse-graining of only the displacement field via selection of representative atoms. The potential fields are computed on the fine-mesh, i.e.  $T_{h_3} = T_{h_2}$ , and the coarse-graining of corrector potential fields is suppressed. This study shows the approximation errors arising solely from coarse-graining of the displacement field. In the second study, along with coarse-graining of the displacement field, corrector fields are also represented using a coarse-grained triangulation. In other words, we consider  $T_{h_3}$  also to be a coarse-grained triangulation with subatomic resolution close to regions of interest and coarse-grained elsewhere. The approximation errors in this study arise from the coarse-graining of the displacement field as well as corrector fields. In the first two studies we do not introduce the quadrature rules proposed in equation (72). The third and final study introduces the quadrature rules as an additional approximation which then reduces all computations to the complexity commensurate with the coarse-grained triangulations  $T_{h_1}$  and  $T_{h_3}$ . The approximation errors in the third study

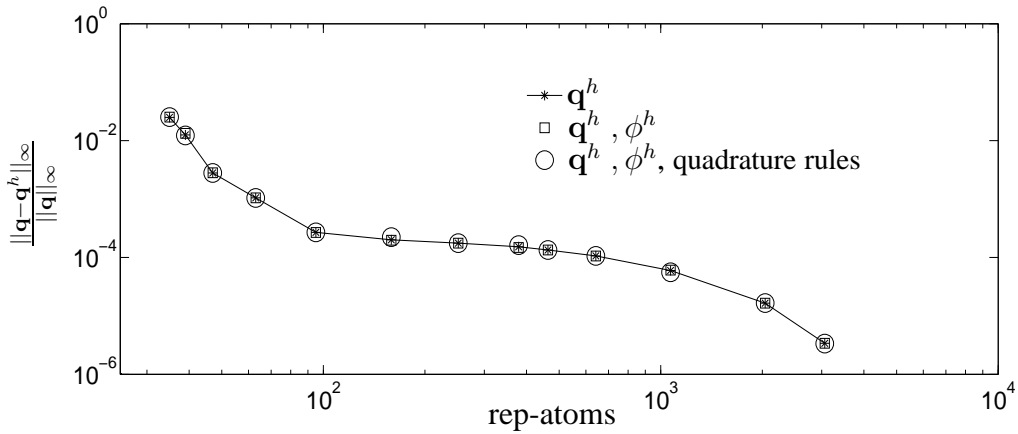
include the coarse-graining errors from displacement and corrector fields, and the quadrature errors.

We have conducted the aforementioned three studies for the set of triangulations given by  $\mathcal{X}^h = \{35, 39, 47, 63, 95, 159, 251, 379, 463, 642, 1069, 3029, 3063\}$ —similar to the set used in the study of approximation errors in the formulation proposed in [Knap & Ortiz \(2001\)](#). Figure 16 shows the approximation errors in displacement field and energy for the three studies with increasing number of rep-atoms. The data points from the first study, denoted by ‘\*’, show the displacement coarse-graining errors which are similar to the displacement coarse-graining errors for the node-based formulation in [Knap & Ortiz \(2001\)](#) (cf. figure 12). The data points from the second study are denoted by ‘□’, and those from the third study are denoted by ‘○’. From figure 16, it is evident that the approximation errors corresponding to the coarse-graining of corrector fields and quadrature rules are negligible in comparison to the coarse-graining errors in the displacement field. These results are in sharp contrast to the errors incurred in using node-based cluster rules where the quadrature errors are orders of magnitude larger than the coarse-graining errors. We argue that this remarkable improvement in the accuracy of the solution can be attributed to two key features of the quasi-continuum reduction of field theories. Firstly, the quadrature rules proposed in the quasi-continuum reduction of field formulations are element-based quadratures. As demonstrated in section 3, element-based cluster (quadrature) rules are more accurate in comparison to node-based cluster rules. Secondly, and more importantly, the notion of quadrature approximation is a local notion which is compatible with field formulations, and as demonstrated in section 5 satisfies the consistency conditions necessary for systematic convergence of approximations.

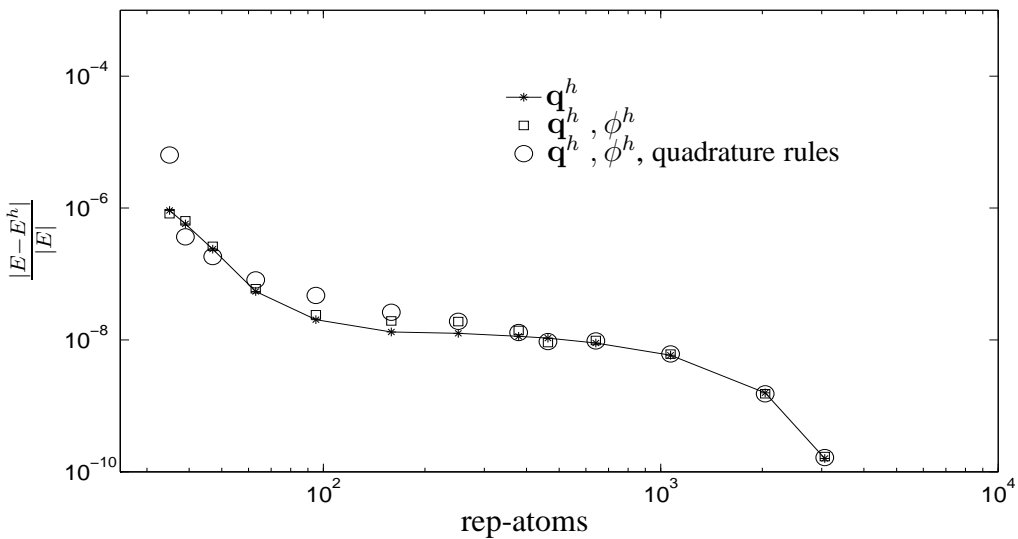
We finally comment on the computational costs associated with the field formulation. As expected, the field formulation has larger memory requirements in comparison to conventional QC formulations as the potential fields have to be resolved on a finite-element mesh at the sub-atomic scale. The memory requirements for the proposed field formulation are  $O(N_{h_1})$  for storing the displacements of the representative atoms, where  $N_{h_1}$  denotes the number of nodes in  $T_{h_1}$ ;  $O(N_{h_3})$  for storing the corrector fields, where  $N_{h_3}$  denotes the number of nodes in  $T_{h_3}$ ; and  $O(N_{h_1} * N_U)$  for storing the predictor fields, where  $N_U$  is the number of nodes in the triangulation of a unit cell. The computational complexity of the force calculation is  $O(N_{h_3}^{\text{e-super}} + N_{h_1})$  once the potential fields are computed for a given configuration of atoms, where  $N_{h_3}^{\text{e-super}}$  denotes the number of superatomic elements in  $T_{h_3}$ . We note that computing potential fields is mostly an overhead cost as it is the initial computation of these fields which is time consuming, and the subsequent evaluations are updates which require very few iterations. In comparison, the memory requirements of conventional QC formulations are  $O(N_{h_1})$ , and the computational complexity of force evaluations is  $O(N_{h_1} * N_{r_c} * N_{r_{\text{cutoff}}})$  where  $N_{r_c}$  denotes the number of atoms inside the cluster radius and  $N_{r_{\text{cutoff}}}$  denotes the number of atoms inside the chosen cut-off radius for the interatomic interactions. For a representative calculation with 95 rep-atoms, the data arrays representing the predictor fields and corrector fields had 18786 entries and 21582 entries respectively, in addition to the displacements of the 95 rep-atoms. The memory requirement for this calculation was about 0.5 MB as opposed to negligible memory



(a) Relative root mean squared error in displacement field



(b) Relative supremum error in displacement field



(c) Relative error in total energy

Fig. 16. Relative approximation errors in displacement field and energy for the proposed field formulation of quasi-continuum method.  $\mathbf{q}^h$  represents coarse-grained displacement field while  $\phi^h$  represents coarse-grained potential field.

requirements for conventional formulations. For a comparison of the computational time, we consider a 95 rep-atom conventional QC formulation with node-based cluster rules on forces with a cluster radius of 20. For this test case, the field formulation consumed four times more wall clock time than the conventional QC formulation with node-base cluster rules. We note that there is significant room for optimization of the field formulation, and by using multi-grid methods the computational complexity of the potential field calculations can be further reduced, which is a topic for future investigation.

## 7 Conclusions

We have presented a solution to some of the long standing issues in the quasi-continuum method. The approximations involved in various versions of the QC method are known to result in undesirable features, which include a loss of variational structure leading to non-conservative forces, appearance of spurious forces on a perfect periodic lattice, possible lack of stability in the numerical approximations, etc. These in turn can undermine the numerical accuracy and systematic convergence of the QC method. In the present work, we identified the primary cause of these shortcomings to be the use of a non-local representation of energy to describe the extended interatomic interactions in materials. We have demonstrated that cluster summation rules introduced on a non-local representation of energy result in a lack of consistency—approximation errors do not systematically reduce with increasing refinement of the solution space. Cluster summation rules which are introduced in the spirit of numerical quadratures are derived from a local notion of numerical approximation, and result in inconsistent schemes when used on non-local representations of energy.

In the present work, we resolved these outstanding issues by reformulating the extended interatomic interactions into a local variational problem involving potential fields. We have demonstrated this approach for commonly used interatomic potentials, and subsequently introduced the quasi-continuum reduction of these potential fields following the ideas first suggested in [Gavini et al. \(2007\)](#) in the context of electronic structure calculations. The key ideas behind the quasi-continuum reduction of field theories are: (i) decomposition of potential fields into predictor fields and corrector fields; (ii) an efficient representation of these fields using nested finite-element triangulations—predictor fields are resolved on an auxiliary unit cell, whereas corrector fields are represented on a coarse-grained triangulation; (iii) introduction of quadrature rules which reduce all computations to the complexity commensurate with the number of coarse-grained variables in the system. We have demonstrated that the quasi-continuum reduction of a field formulation satisfies the necessary conditions for a consistent numerical approximation, and hence is likely to provide a systematic convergence of the approximation errors. Further, we have shown using numerical examples the remarkable improvement in the accuracy of the solution afforded by the suggested field approach to the QC method. Numerical results from this study suggest that the approximation errors in a field approach are solely from the coarse-graining of displacement fields which can not be surpassed by any QC

formulation. In comparison, other seamless QC formulations based on non-local representations of energy incur orders of magnitude larger numerical errors from quadrature approximations, and also suffer from a lack of systematic convergence.

The suggested field theoretic approach to the quasi-continuum method has the following properties. A single field theory is used to describe the physics in all regions of the model. The formulation is seamless and does not rely on any patching conditions. The formulation has a variational structure and thus the computed forces are conservative. The approximations introduced are consistent, and hence provide a systematic convergence to the exact solution. Moreover, the present work provides a general framework for the quasi-continuum reduction of any field theory, where quasi-continuum reduction is solely a numerical coarse-graining technique.

It may appear that the computation of potential fields, which requires resolving these fields on a length-scale finer than interatomic distance, can significantly increase the computational cost. We note that the computation of these potential fields is mostly an overhead cost as it is the initial computation of these fields which is time consuming, and the subsequent evaluations are updates which require very few iterations. On the other hand, the field formulation provides a significant advantage as the computation of forces and energy is a local computation involving the potential fields, unlike force and energy computations in conventional QC formulations. In our simulations, the field formulation was about four times more expensive in computational time than conventional node-based formulations. However, there is significant room for optimization in our preliminary implementation of the field formulation. For instance, the use of multi-grid approaches can significantly reduce the computational complexity of potential field calculations.

In the present work we have restricted our attention to a single component material system. Extending the present ideas to multi-component systems requires careful consideration as the PDE's describing potential fields can have different forms in different regions of the model, and presents itself as a direction for future investigations. Further, a numerical analysis of the proposed method which includes developing *a priori* error estimates, investigating the stability and accuracy of the formulation, developing effective preconditioned iterative solvers are potential directions for future investigations.

## **Acknowledgements**

We thank Prof. Liping Liu and Dr. Christoph Ortner for useful discussions on this work. The financial support of Air Force Office of Scientific Research under Grant No. FA9550-09-1-0240 is gratefully acknowledged. V.G. also gratefully acknowledges the research grant from the Horace. H. Rackham School of Graduate studies at University of Michigan.

**References**

- Ashcroft, N.W., Mermin, N. D., 1976. *Solid State Physics*, Brooks Cole Publishing.
- Blanc, X., Le Bris, C., Lions, P.L., 2002. From molecular models to continuum mechanics. *Arch. Rational Mech. Anal.* 164, 341-381.
- Boyd, S., Vandenberghe, L., 2004. *Convex Optimization*, Cambridge University Press, Cambridge.
- Curtin W.A, Miller, R.E, 2003. Atomistic/continuum coupling in computational materials science, *Modelling Simul. Mater. Sci. Eng.* 11, R33-R68.
- Dacorogna, B., 1989. *Direct Methods in the Calculus of Variations*, Applied Mathematical Sciences, Volume 78, Springer-Verlag, Berlin, Heidelberg, New York.
- Daw, M.S., Baskes, M.I., 1984. Embedded-atom method: derivation and application to impurities, surfaces, and other defects in metals. *Phys. Rev. B* 29, 6443-6453.
- Dobson, M., Luskin, M., 2009. An optimal order error analysis of the one-dimensional quasicontinuum approximation. *SIAM J. Numer. Anal.* 47, 2455-2475.
- Dobson, M., Luskin, M., Ortner, C., 2009. Stability, instability, and error of the force-based quasicontinuum approximation. *Archive for Rational Mechanics and Analysis*, to appear. arXiv:0903.0610.
- Dobson, M., Luskin, M., Ortner, C., 2010a. Sharp Stability Estimates for Force-based Quasicontinuum Methods, *SIAM J. Multiscale Modeling & Simulation*, to appear. arXiv:0907.3861.
- Dobson, M., Luskin, M., Ortner, C., 2010b. Accuracy of Quasicontinuum Approximations Near Instabilities, arXiv:0905.2914
- E, W., Lu, J., Yang, J.Z., 2006. Uniform accuracy of the quasicontinuum method. *Phys. Rev. B* 74, 214115.
- Eidel, B., Stukowski, A., 2009. A variational formulation of the quasicontinuum method based on energy sampling in clusters. *J. Mech. Phys. Solids.* 57, 87-108.
- Finnis, M., 2003. *Interatomic forces in condensed matter*, Oxford University Press Inc., Oxford, New York.
- Gavini, V., Bhattacharya, K., Ortiz, M., 2007. Quasi-continuum orbital-free density-functional theory: A route to multi-million atom non-periodic DFT calculation. *J. Mech. Phys. Solids.* 55, 697-718.
- Gavini, V., Liu, L., 2010. An analysis of the field theoretic approach to quasi-continuum method. *J. Mech. Phys. Solids.* (submitted).
- Gunzburger, M., Zhang, Y., 2009. A quadrature-rule type approximation for the quasicontinuum method. *Multiscale Model. Sim.*, to appear.
- Johnson, R.A., 1988. Analytic nearest-neighbor model for fcc metals. *Phys. Rev. B* 37, 3924-3931.
- Jones, J.E., 1924. On the determination of molecular fields. II. From the equation of state of a gas, *Proc. R. Soc. Lond. A* 106, 463-477.
- Knap, J., Ortiz, M., 2001. An analysis of the quasicontinuum method. *J. Mech. Phys. Solids.* 49, 1899-1923.
- Knap, J., Ortiz, M., 2003. Effect of indenter-radius size on Au (0 0 1) nanoindentation. *Phys. Rev. Lett.* 90, 226102.
- Luskin, M., Ortner, C., 2009. An analysis of node-based cluster summation rules in the

- quasicontinuum method. *SIAM J. Numer. Anal.* 47, 3070-3086.
- Miller, R., Ortiz, M., Phillips, R., Shenoy, V., Tadmor, E.B. 1998a. Quasicontinuum models of fracture and plasticity. *Eng. Fract. Mech.* 61, 427-444.
- Miller, R., Tadmor, E.B., Phillips R., Ortiz, M., 1998b. Quasicontinuum simulation of fracture at the atomic scale. *Modelling Simul. Mater. Sci. Eng.* 6, 607-638.
- Miller, R.E., Tadmor, E.B., 2002. The quasicontinuum method: overview, applications and current directions. *J. Comput. Aided Mater. Des.* 9, 203-239.
- Miller, R.E., Tadmor, E.B., 2009. A Unified Framework and Performance Benchmark of Fourteen Multiscale Atomistic/Continuum Coupling Methods. *Model. Sim. Mat. Sci. Eng.* 17, 053001.
- Ming, P., Yang, Z., 2009. Analysis of a one-dimensional nonlocal quasi-continuum method. *Multiscale modelling and simulation* 7, 1838-1875.
- Moré, J.J., "The Levenberg-Marquardt Algorithm: Implementation and Theory," *Numerical Analysis*, ed. G. A. Watson, *Lecture Notes in Mathematics* 630, Springer Verlag, pp 105-116, 1977.
- Phillips, R., Rodney, D., Shenoy, V., Tadmor, E.B., Ortiz, M., 1999. Hierarchical models of plasticity: dislocation nucleation and interaction. *Modelling Simul. Mater. Sci. Eng.* 7, 769-780.
- Morse, P.M., 1929. Diatomic molecules according to the wave mechanics. II. Vibrational levels. *Phys. Rev.* 34, 57-64.
- Ortiz, M., Phillips, R., 1999. Nanomechanics of defects in solids. *Adv. Appl. Mech.* 36, 1-79.
- Shenoy, V.B., Miller, R., Tadmor, E.B., Rodney, D., Phillips, R., Ortiz, M., 1999. An adaptive finite element approach to atomic-scale mechanics—the quasicontinuum method. *J. Mech. Phys. Solids* 47, 611-642.
- Shenoy, V.B., Phillips R., Tadmor, E.B., 2000. Nucleation of dislocations beneath a plane strain indenter. *J. Mech. Phys. Solids* 48, 649-673.
- Shimokawa, T., Mortensen, J.J., Schiøtz, J., Jacobsen, K.W., 2004. Matching conditions in the quasicontinuum method: removal of the error introduced at the interface between the coarse-grained and fully atomistic region. *Phys. Rev. B* 69, 214104.
- Strang, G.W, Fix, G.J., 1973. *An analysis of the finite element method*, Wellesley Cambridge Press.
- Sutton, A.P., Chen, J., 1990. Long range Finnis-Sinclair potentials. *Phil. Mag. Lett.* 61, 139-146.
- Tadmor, E.B., Ortiz, M., Phillips, R., 1996a. Quasicontinuum analysis of defects in solids. *Philos. Mag.* 73, 1529-1563.
- Tadmor, E.B., Phillips, R., Ortiz, M., 1996b. Mixed atomistic and continuum models of deformation in solids. *Langmuir* 12, 4529-4534.
- Tadmor, E.B., Miller, R., Phillips R., Ortiz, M., 1999. Nanoindentation and incipient plasticity. *J. Mater. Res.* 14, 2233-2250.

## A Error Estimates

For completeness we provide the details of the estimate in equation (38) that corresponds to the error in the computation of forces using element-based cluster summations. Following the notation introduced in section 3.2 and 3.3 we denote  $g(k) = \sum_{j \in \mathcal{L}} \bar{K}'(x_k - x_j) \frac{x_k - x_j}{|x_k - x_j|} \Phi^h(X_j | X_0)$ ,  $k_1(i) = \frac{Ny}{2} - i$  and  $k_2(i) = \frac{N}{2} - i$  which for  $i = -r_0 \dots r_0$  denote the positions of the atoms in the clusters located in the two elements shown in figure 4. The expressions for  $g(k_1(i))$  and  $g(-k_2(i))$  for  $i \in \{-r_0, \dots, r_0\}$  are given by

$$\begin{aligned}
 g(k_1(i)) &= \sum_{j=k_1(i)+1}^{Ny} \bar{K}'(a_1|k_1(i) - j) \frac{Ny - j}{Ny} - \left\{ \sum_{j=0}^{k_1(i)-1} \bar{K}'(a_1|k_1(i) - j) \frac{Ny - j}{Ny} \right. \\
 &\quad \left. + \sum_{j=1}^N \bar{K}'(a_1|k_1(i) + j) \frac{N - j}{N} \right\} \quad i = -r_0 \dots r_0, \\
 g(-k_2(i)) &= - \sum_{j=k_2(i)+1}^N \bar{K}'(a_1|k_2(i) - j) \frac{N - j}{N} + \left\{ \sum_{j=0}^{k_2(i)-1} \bar{K}'(a_1|k_2(i) - j) \frac{N - j}{N} \right. \\
 &\quad \left. + \sum_{j=1}^{Ny} \bar{K}'(a_1|k_2(i) + j) \frac{Ny - j}{Ny} \right\} \quad i = -r_0 \dots r_0.
 \end{aligned} \tag{A.1}$$

The approximate force on representative node  $K = 0$  is given by

$$\tilde{f}_0 = \sum_{i=-r_0}^{r_0} \left( \frac{Ny}{2r_0 + 1} g(k_1(i)) + \frac{N}{2r_0 + 1} g(-k_2(i)) \right). \tag{A.2}$$

From symmetry we note that

$$\begin{aligned}
 \sum_{i=-r_0}^{r_0} \left( \sum_{j=k_1(i)+1}^{Ny} \bar{K}'(a_1|k_1(i) - j) - \sum_{j=0}^{k_1(i)-1} \bar{K}'(a_1|k_1(i) - j) \right) &= 0. \\
 \sum_{i=-r_0}^{r_0} \left( \sum_{j=0}^{k_2(i)-1} \bar{K}'(a_1|k_2(i) - j) - \sum_{j=k_2(i)+1}^N \bar{K}'(a_1|k_2(i) - j) \right) &= 0.
 \end{aligned} \tag{A.3}$$

Using equation (A.3) in equation (A.1) and rearranging, the approximate force is given by

$$\begin{aligned}
 \tilde{f}_0 &= \sum_{i=-r_0}^{r_0} \frac{1}{2r_0+1} \left( z(k_1(i)) - z(k_2(i)) + N \sum_{j=1}^{Ny} \bar{K}'(a_1|j+k_2(i)|) - Ny \sum_{j=1}^N \bar{K}'(a_1|j+k_1(i)|) \right), \\
 z(k_1(i)) &= \sum_{j=0}^{k_1(i)-1} \bar{K}'(a_1|j-k_1(i)|)j - \sum_{j=k_1(i)+1}^{Ny} \bar{K}'(a_1|j-k_1(i)|)j + y \sum_{j=1}^N \bar{K}'(a_1|j+k_1(i)|)j, \\
 z(k_2(i)) &= \sum_{j=0}^{k_2(i)-1} \bar{K}'(a_1|j-k_2(i)|)j - \sum_{j=k_2(i)+1}^N \bar{K}'(a_1|j-k_2(i)|)j + \frac{1}{y} \sum_{j=1}^{Ny} \bar{K}'(a_1|j+k_2(i)|)j.
 \end{aligned} \tag{A.4}$$

which is equation (38). To simplify this expression we make a series of approximations. First we choose clusters containing only one atom, which corresponds to  $r_0 = 0$ . Further for simplicity we will drop the terms of  $O(\frac{1}{(3N)^p})$  in comparison to terms of  $O(\frac{1}{N^p})$ . Lastly, we assume  $y = 1 + \epsilon$  with  $\epsilon > 0$  and  $\epsilon \ll 1$ . Using the decay assumption on  $\bar{K}$  in assumption A1 (section 3) and properties of p-series noted in section 3.1, we arrive at the following estimates

$$\begin{aligned}
 N \sum_{j=1}^{Ny} \bar{K}'(a_1|j+k_2(i)|) - Ny \sum_{j=1}^N \bar{K}'(a_1|j+k_1(i)|) &\approx \frac{2(p-1)\epsilon}{pa_1^{p+1}(\frac{N}{2})^{p-1}}, \\
 y \sum_{j=1}^N \bar{K}'(a_1|j+k_1(i)|)j - \frac{1}{y} \sum_{j=1}^{Ny} \bar{K}'(a_1|j+k_2(i)|)j &\approx \frac{(3-p)\epsilon}{p(p-1)a_1^{p+1}(\frac{N}{2})^{p-1}}, \\
 \sum_{j=0}^{k_1(i)-1} \bar{K}'(a_1|j-k_1(i)|)j - \sum_{j=0}^{k_2(i)-1} \bar{K}'(a_1|j-k_2(i)|)j \\
 + \sum_{j=k_2(i)+1}^N \bar{K}'(a_1|j-k_2(i)|)j - \sum_{j=k_1(i)+1}^{Ny} \bar{K}'(a_1|j-k_1(i)|)j &\approx \frac{4\epsilon}{a_1^{p+1}(\frac{N}{2})^{p-1}}.
 \end{aligned} \tag{A.5}$$

Using the estimates in (A.5), we note that  $\tilde{f}_0$  is  $O(\frac{y-1}{N^{p-1}})$ .